Nitrogen and carbon dynamics in the Scheldt estuary at the beginning of the 21st century ? a modelling study

A. F. Hofmann, K. Soetaert, J. J. Middelburg

▶ **To cite this version:**

A. F. Hofmann, K. Soetaert, J. J. Middelburg. Nitrogen and carbon dynamics in the Scheldt estuary at the beginning of the 21st century ? a modelling study. Biogeosciences Discussions, 2008, 5 (1), pp.83-161. hal-00297958

HAL Id: hal-00297958
https://hal.science/hal-00297958

Submitted on 18 Jun 2008

HAL is a multi-disciplinary open access archive for the deposit and dissemination of scientific research documents, whether they are published or not. The documents may come from teaching and research institutions in France or abroad, or from public or private research centers.

L'archive ouverte pluridisciplinaire **HAL**, est destinée au dépôt et à la diffusion de documents scientifiques de niveau recherche, publiés ou non, émanant des établissements d'enseignement et de recherche français ou étrangers, des laboratoires publics ou privés.

Biogeosciences Discuss., 5, 83–161, 2008
www.biogeosciences-discuss.net/5/83/2008/
© Author(s) 2008. This work is licensed
under a Creative Commons License.

Biogeosciences Discussions

Biogeosciences Discussions is the access reviewed discussion forum of *Biogeosciences*

Nitrogen and carbon dynamics in the Scheldt estuary at the beginning of the 21st century – a modelling study

A. F. Hofmann, K. Soetaert, and J. J. Middelburg

Netherlands Institute of Ecology (NIOO-KNAW), Centre for Estuarine and Marine Ecology – P.O. Box 140, 4400 AC Yerseke, The Netherlands

Received: 19 November 2007 – Accepted: 2 December 2007 – Published: 11 January 2008

Correspondence to: A. F. Hofmann (a.hofmann@nioo.knaw.nl)

Abstract

A 1-D, pelagic, reactive-transport model of a completely mixed, turbid, heterotrophic estuary – the Scheldt estuary – is presented. The model contains major carbon and nitrogen species and oxygen, as well as pH. The model features three organic matter degradation pathways, oxic mineralisation, denitrification and sulfate reduction, and includes nitrification and sulfide re-oxidation. Apart from advective-dispersive transport along the length axis, the model also describes O_2, CO_2, NH_3, and N_2 air-water exchange. The aim of this model exercise is to determine the fate and turnover of nutrients entering the estuary and their spatial patterns at the beginning of the 21st century. Nitrification is identified as one of the most important processes in the estuary, consuming with 1.7 Gmol $O_2\,y^{-1}$ more oxygen than oxic mineralisation (1.4 Gmol $O_2\,y^{-1}$). About 8% of the 2.4 Gmol of nitrogen entering the estuary per year is lost within the estuary due to denitrification. Nitrogen and carbon budgets are compared to budgets from the seventies and eighties, showing that nitrification activity has peaked in the eighties, while denitrification steadily declined. Our model estimates an average of 3.6 Gmol y^{-1} of CO_2 export to the atmosphere in the years 2001 to 2004, which is a comparatively low estimate in the context of previous estimates of CO_2 export from the Scheldt estuary.

1 Introduction

Estuaries play an important role in the transfer of land derived nutrients and organic matter to the coastal ocean as they act as bio-reactors where both the quantity and the quality of the constituents are altered Soetaert et al. (2006). Additionally, Borges et al. (2006) and Frankignoulle et al. (1998) report that estuaries are globally important sources of CO_2, by ventilating riverine dissolved inorganic carbon (DIC) as well as DIC originating from the degradation of riverine organic matter. This estuarine filter function is not a static property and evolves with changing forcings (Cloern, 2001).

BGD

5, 83–161, 2008

Thorough assessment of evolving estuarine filter functioning requires not only access to long-term datasets documenting changes in concentrations and loadings, but also biogeochemical models that allow reproducing these trends and deriving transformation intensities.

Long term changes in estuarine biogeochemical cycling have been well documented for the Scheldt estuary (Soetaert et al., 2006). Billen et al. (1985) predicted that increased oxygen levels due to lowered organic loadings would increase delivery of nitrogen to the North Sea. Soetaert and Herman (1995a) indeed found that in the eighties an increased percentage of riverine nitrogen was exported to the North Sea as compared to the seventies. Recently, Soetaert et al. (2006) report major changes for the Scheldt estuary, not only in nutrient loadings, but also changes in nitrogen and phosphorus retention and regeneration, from the mid sixties to the beginning of the 21st century. Against this background it is of interest to investigate the interplay of different biogeochemical processes as well as to quantify import and export of constituents to both the North Sea and the atmosphere in the Scheldt estuary at the beginning of the 21st century.

For macrotidal estuaries as the Scheldt estuary, Vanderborght et al. (2007) identify reactive-transport modelling as a powerful approach to investigate nutrients and carbon budgets and cycling at the estuarine scale. To answer questions about seasonal dynamics, a fully coupled, two-dimensional hydrodynamic and reactive-transport model (e.g. Vanderborght et al., 2007) is the method of choice. However, for the assessment of an average situation for a certain period of time that can be compared to other decades, a simple 1-D model reproducing yearly averaged values is sufficient (cf. also 1-D approaches by Soetaert and Herman, 1994, 1995a,b,c; Regnier et al., 1997).

The objective of this study was to construct a 1-D, biogeochemical, pelagic, reactive-transport model of the mixed, turbid, heterotrophic Scheldt estuary. The model contains major carbon and nitrogen species and oxygen, as well as pH. The model is deliberately kept rather simple to optimize the ratio between the number of parameters and data available for calibration and validation. We use this model to determine the fate

and turnover of nutrients entering the estuary and to describe the spatial patterns of nutrient concentrations and fluxes in the Scheldt estuary at the beginning of the 21st century. We derive budgets and fluxes for nitrogen and compare those to budgets from the seventies (Billen et al., 1985) and eighties (Soetaert and Herman, 1995a). The obtained value for an average CO_2 export to the atmosphere in the years 2001 to 2004 will be compared to reported CO_2 water-air flux estimates for the Scheldt estuary (Frankignoulle et al., 1998; Gazeau et al., 2005; Hellings et al., 2001; Vanderborght et al., 2002).

2 Materials and methods

2.1 The scheldt estuary

The Scheldt estuary is situated in the southwest Netherlands and northern Belgium (Fig. 1). The roughly 350 km (Soetaert et al., 2006; Van Damme et al., 2005) long Scheldt river drains a basin of around 21 500 km^2 (average from numbers given in Soetaert et al., 2006, Vanderborght et al., 2007, Van Damme et al., 2005 and Meire et al., 2005) located in the northwest of France, the west of Belgium and the southwest of the Netherlands (Soetaert et al., 2006). The hydrographical basin of the Scheldt contains one of the most densely populated areas in Europe (Vanderborght et al., 2007) with about 10 million inhabitants (Meire et al., 2005; Soetaert et al., 2006), resulting in an average of 465 inhabitants per km^2. Anthropogenic eutrophication and pollution of the Scheldt estuary therefore are of considerable magnitude, especially due to the poor waste water treatment in upstream areas, e.g. in Brussels (Meire et al., 2005; Van Damme et al., 2005; Soetaert et al., 2006; Vanderborght et al., 2007). The water movement in the Scheldt estuary is dominated by huge tidal displacements with around 200 times more water entering the estuary during a flood than the freshwater discharge during one tidal cycle (Vanderborght et al., 2007). The average freshwater flow is around 100 $m^3 s^{-1}$ (Heip, 1988). The cross sectional area of the estuarine channel

shows a quite regular trumpet-like shape opening up from around 4000 m^2 upstream to around 75 000 m^2 downstream (Fig. 2; Soetaert et al., 2006) whilst the mean water depth varies quite irregularly between values of 6 m and 14 m with the deepest areas towards the downstream boundary (Soetaert and Herman, 1995b). The estuary has a total tidally averaged volume of about 3.619×10^9 m^3 and a total tidally averaged surface area of 338 km^2 (Soetaert et al., 2006; Soetaert and Herman, 1995b), the major parts of which are situated in the downstream area. Peters and Sterling (1976), as cited by Vanderborght et al. (2007), divide the Scheldt river into three zones: The first zone, between the estuarine mouth at Vlissingen and Walsoorden, consists of a complex system of flood and ebb channels and a moderate longitudinal salinity gradient within the polyhaline range. The second zone from Walsoorden to Rupelmonde is characterised by a well defined river channel and a steep salinity gradient with salinities at Rupelmonde between 0 and 5 (Meire et al., 2005). The third zone, upstream from Rupelmonde, consists of the Scheldt freshwater river system and various tributaries, with tidal influence in the Scheldt up to the sluices of Gent (Van Damme et al., 2005). The model presented here comprises the first and the second zone with an upstream boundary at Rupelmonde (river km 0) and a downstream boundary at Vlissingen (river km 104).

2.2 Physical-biogeochemical model

2.2.1 Biogeochemical processes

The model describes five main biogeochemical processes, oxic mineralisation ($\mathbf{R}_{Ox}$), denitrification ($\mathbf{R}_{Den}$), sulfate reduction ($\mathbf{R}_{SRed}$), nitrification ($\mathbf{R}_{Nit}$), and sulfate re-oxidation ($\mathbf{R}_{SOx}$) as given in Table 1. Due to the highly heterotrophic and turbid nature of the Scheldt estuary (Soetaert and Herman, 1995c; Gazeau et al., 2005; Soetaert et al., 2006; Vanderborght et al., 2002, 2007), primary production is very limited (much lower than respiration in Gazeau et al. (2005) and one order of magnitude lower than respiration in Vanderborght et al., 2002), mainly restricted to the freshwater tidal reaches

(Arndt et al., 2007), and is therefore not considered in the model. Oxic mineralisation and denitrification are included as the two pathways of organic matter degradation that are energetically most favourable (Canfield et al., 2005). Reduction of manganese and iron oxyhydroxides is neglected because of their low concentrations. However, sulfate reduction is included in the model. Consequently, also re-oxidation of sulfide should be part of the model. Nitrification is included in the model since it is one of the most important O_2 consuming processes in the Scheldt estuary (Soetaert and Herman, 1995a; Andersson et al., 2006).

Denitrification follows traditional stoichiometry because of its limited importance (at present) and the absence of data on Anammox (anaerobic ammonium oxidation).

Table 2 shows kinetic formulations for all processes considered in the model. As in Soetaert and Herman (1995a), organic matter has been split up into two different fractions, one fast decaying fraction FastOM with a low C/N-ratio of γ_{FastOM} and one slow decaying fraction SlowOM with a high C/N-ratio of γ_{SlowOM}, respectively. $\mathbf{R}_{\mathrm{Ox}}$, $\mathbf{R}_{\mathrm{Den}}$ and $\mathbf{R}_{\mathrm{SRed}}$ are modelled as first order processes with respect to organic matter concentration in terms of organic nitrogen as done by Soetaert and Herman (1995a). As in Regnier et al. (1997) and Soetaert and Herman (1995a), oxygen concentration inhibits denitrification and sulfate reduction, whereas nitrate concentration inhibits sulfate reduction in a 1-Monod fashion. Nitrate concentration influences denitrification according to a Monod relationship as given by Regnier et al. (1997). The molecular nitrogen produced by denitrification is assumed to be immediately lost to the atmosphere. Mineralisation processes are thus modelled in the same order of sequence as in diagenetic models, depending on the availability of different oxidants with different free energy yields per mole organic matter oxidised (e.g. Froelich et al., 1979; Canfield et al., 2005; Soetaert et al., 1996). Note that denitrification in our model is, although pelagically modelled, a proxy for benthic denitrification. Therefore, the parameters $k^{\mathrm{Inh}}_{\mathrm{O_2}}$ and $k_{\mathrm{NO_3^-}}$ should not be considered true microbiological rate parameters.

Total mineralisation rates for fast and slow degrading organic matter are assumed

to be only dependent on temperature and not on the mineralisation pathway. To ensure that the total temperature dependent mineralisation rates rt_X^{Min}, for FastOM and SlowOM respectively, are always realised, the independently calculated limitation factors for all three potentially simultaneously occurring mineralisation processes are rescaled as in Soetaert et al. (1996) to partition the total mineralisation rates.

Nitrification is expressed as a first order process with respect to ammonium concentration and with a Monod dependency on oxygen as in Soetaert et al. (1996). The same oxygen half saturation parameter k_{O_2} as for oxic mineralisation is used for nitrification. Nitrification may depend on the microbial community of nitrifiers. de Bie et al. (2001) documented dramatic shifts in nitrifier populations along the estuary from the freshwater to the marine part. Therefore, we assume that the nitrification activity in the freshwater (upstream) part of the modelled system is performed by freshwater nitrifying organisms that experience increasing stress as salinity increases. As a consequence, their activity collapses in the downstream region due to an insufficient adaptation to marine conditions (see also Helder and Devries, 1983) which is incompletely compensated by activity of marine nitrifying species, so that the overall nitrification activity in the estuary decreases with increasing salinity. This is expressed with an inverse dependency of nitrification on salinity, according to a sigmoid function based on a Holling Type III functional response (Gurney and Nisbet, 1998), modified to have a value of 1 for zero salinity and to asymptotically reach an offset value of o^{Nit} for high salinities.

Re-oxidation of sulfide is modelled as a first order process with respect to $[\sum H_2S]$, the same maximal rate and oxygen inhibition formulation as for nitrification are used.

The temperature dependency for all processes is modelled with a Q_{10} formulation using a standard Q_{10} value of 2, all rates are expressed at a standard base temperature of 15°C.

Values for k_{O_2}, $k^{Den}_{NO_3^-}$ and $k^{Inh}_{NO_3^-}$ are taken from Regnier et al. (1997), values for $k^{Inh}_{O_2}$, r^{Min}_{SlowOM}, γ_{FastOM} and γ_{SlowOM} are taken from Soetaert and Herman (1995a) ($k^{Inh}_{O_2}$, γ_{FastOM} and γ_{SlowOM} have been rounded). The parameters r^{Min}_{FastOM}, r^{Nit}, p, k_S^{Inh} and o^{Nit}

have been calibrated.

2.2.2 Acid-base reactions (equilibria)

In any natural aqueous system, and in saline systems in particular, a certain set of chemical acid-base reactions has to be taken into account if pH is to be modelled. Due to their fast reaction rates compared to all other modelled processes, these reversible acid-base reactions are considered to be in local equilibrium at any time and at any point in the estuary (Stumm and Morgan, 1996). For the model presented here, the set of acid-base equilibria given in Table 3 is chosen.

2.2.3 Physical processes

Air-water exchange

While N_2 is assumed to be instantaneously lost to the atmosphere, O_2, CO_2, and NH_3 are exchanged with the atmosphere according to a formulation given in Thomann and Mueller (1987):

$$\mathbf{E}_C = \left.\frac{d[C]}{dt}\right|_{\text{Air-Sea}} = K_{L_C}\frac{A}{V}([C]_{sat}-[C]) = \frac{K_{L_C}}{D}([C]_{sat}-[C]) \quad (1)$$

with [C] (mmol m^{-3}) signifying the actual concentration of O_2, CO_2, or NH_3, respectively, $[C]_{sat}$ (mmol m^{-3}) being the saturation concentration of chemical species C in the water. K_{L_C} (m d^{-1}) is the piston velocity, A (m^2) the horizontal surface area of the model box in question, V (m^3) the volume, and D (m) the mean water depth.

Saturation concentrations are calculated using Henry's law (e.g. Atkins, 1996):

$$[C]_{sat} = fC\, K_{0_C}\, \rho_{SeaWater} \quad (2)$$

with fC (atm) being the fugacity of C, K_{0_C} (mmol (kg-soln atm)$^{-1}$) being the Henry's constant for C, and $\rho_{SeaWater}$ (kg-soln m^{-3}) being the temperature and salinity dependent density of seawater. Henry's constants are calculated according to Weiss (1974) for CO_2 and based on Weiss (1970) for O_2. Both formulations can be found in appendix B1. The atmospheric fugacities of CO_2 and O_2 are assumed to be the same as their atmospheric partial pressures. fCO_2 over the Scheldt waters is assumed to be 383 μatm (averaged from Scheldt area specific values for pCO_2 (partial pressure) given in Borges et al., 2004b), fO_2 is assumed[1] to be 0.20946 atm as given by Williams (2004). The temperature and salinity dependent density of seawater is calculated according to Millero and Poisson (1981). The saturation concentration of NH_3 is assumed constant at 10^{-4} mmol m^{-3}. It is estimated using a Henry's constant of 17.6 mmol m^{-3} atm^{-1} for NH_3 obtained from Plambeck (1995) and an assumed atmospheric pNH_3 of 5.7 n atm, as given by Sakurai et al. (2003).

The piston velocities K_{L_C} are strongly dependent on wind speed. A variety of different empirical relationships between K_{L_C} and wind speed have been proposed in the literature (e.g. Wanninkhof, 1992; Borges et al., 2004b; Raymond and Cole, 2001; McGillis et al., 2001; Clark et al., 1995; Liss and Merlivat, 1986; Kuss et al., 2004; Nightingale et al., 2000; Banks and Herrera, 1977; Kremer et al., 2003). All these relationships have been implemented and tested. For our model, a scaled version of the formulation given by Borges et al. (2004b), which is especially devised for estuaries and the Scheldt estuary in particular, and which includes the effect of estuarine tidal current velocity, was found to produce the best results. For CO_2 this formulation is standardised to a Schmidt number of 600 (i.e. the Schmidt number of CO_2 in freshwater at 20°C) and for O_2 it is assumed be standardised to a Schmidt number of 530 (i.e. the Schmidt number of O_2 in freshwater at 20°C). It is converted to a salinity and temperature dependent value using the formulations for temperature dependent CO_2 and O_2 Schmidt numbers

[1] considering an ambient pressure of 1 atm and considering the density of O_2 to be the same as the density of air, and assuming $fO_2 \approx pO_2$

for freshwater (salinity 0) and seawater (salinity 35) given in Wanninkhof (1992), into which salinity dependency has been incorporated by linear interpolation as described in Borges et al. (2004b). To obtain an adequate fit between model and data for pH and $[O_2]$, the piston velocity for all three species has been scaled by a factor s_{pist}=0.25. Appendix B2 gives K_{L_C} formulations for O_2, CO_2 and NH_3. $K_{L_{NH_3}}$ is assumed to be equal to $K_{L_{CO_2}}$.

Advective-dispersive transport

Since this model focuses on a period of several years, tidally averaged one-dimensional advective-dispersive transport of substances (all modelled substances/chemical species are assumed to be dissolved) is assumed. This transport approach incorporates longitudinal dispersion coefficients which parametrise a variety of physical mechanisms, including effects of either vertical or horizontal shear in tidal currents (Monismith et al., 2002). Advective-dispersive transport $\mathbf{Tr}_C$ of chemical species C is expressed as given in Thomann and Mueller (1987) and used amongst others by Soetaert and Herman (1995b) and Ouboter et al. (1998) for the Scheldt estuary:

$$\mathbf{Tr}_C = \frac{\partial [C]}{\partial t}\bigg|_{\text{Adv-Disp}} = \frac{1}{A}\left(\frac{\partial}{\partial x}\left(E\ A\ \frac{\partial [C]}{\partial x}\right) - \frac{\partial}{\partial x}\left(Q\ [C]\right)\right) \quad (3)$$

The cross sectional area of the channel A (m^2), the tidal dispersion coefficient E ($m^2\ s^{-1}$) and the advective flow Q ($m^3\ s^{-1}$) are functions of the position x along the estuary. Due to the lack of experimental data for E in the Scheldt estuary, a relationship between local water depth and E has been developed as part of this work.

The model has been spatially discretised according to a finite differences approach given in Thomann and Mueller (1987). Equation (3) can be spatially discretised for concentrations $[C]_i$ in mmol m^{-3} of any modelled species C in spatial model box i, describing the flow of matter across a set of model boxes with homogeneous contents and constant volume over time. This is done by applying a first order centred differ-

encing scheme with a step-width of half a model box to the dispersive term, first to the "outer" derivative, then to the obtained "inner" derivatives. In the discretisation of the advective term, the same centred differencing scheme is used for the flux Q, while a backwards differencing scheme[2] is used for the concentration [C]. This approach leads to a transport formulation of:

$$\mathbf{Tr}_{\mathrm{C}}|_i \approx \left(E'_{i-1,i}\left([\mathrm{C}]_{i-1}-[\mathrm{C}]_i\right) - E'_{i,i+1}\left([\mathrm{C}]_i - [\mathrm{C}]_{i+1}\right)\right.$$
$$\left. + Q_{i-1,i}[\mathrm{C}]_{i-1} - Q_{i,i+1}[\mathrm{C}]_i \right) \cdot V_i^{-1} \quad (4)$$

with

$$E'_{i-1,i} = E_{i-1,i}\, A_{i-1,i}\, \left(\Delta x_{i-1,i}\right)^{-1} \quad (5)$$

and $Q_{i-1,i}$ ($\mathrm{m^3\,s^{-1}}$) being the flow over the interface between box $i-1$ and i; $E'_{i-1,i}$ ($\mathrm{m^3\,s^{-1}}$) the bulk dispersion coefficient at the interface between box $i-1$ and i; $E_{i-1,i}$ ($\mathrm{m^2\,s^{-1}}$) the tidal dispersion coefficient at the interface between box $i-1$ and i; $A_{i-1,i}$ ($\mathrm{m^2}$) the cross sectional area of the interface between box $i-1$ and i; Δx_i (m) the length of model box i; and $\Delta x_{i-1,i}$ (m) the length from the centre of box $i-1$ to the centre of box i.

2.2.4 Model state variables and their rates of change

The chemical equilibrium reactions happen on a much faster timescale than the biogeochemical and physical processes (Zeebe and Wolf-Gladrow, 2001). To avoid numerical instabilities while keeping the solution of the model computationally feasible, a set of model state variables that are invariant to the acid-base equilibria has been devised.

[2] Using the same centred differencing scheme for concentrations as well would mean calculating concentrations at the boundary of model boxes. This can lead to a non mass conservative behaviour as the example of a zero concentration in the previous model box and a non-zero one in the current model box shows.

This was done using the canonical transformation and operator splitting approach (Hofmann et al., 2007). In short, this approach proceeds as follows.

Based on the biogeochemical processes given in Table 1 and the chemical equilibria given in Table 3, neglecting N_2, adding salinity Sal and dissolved organic carbon (DOC), and splitting organic matter ($(CH_2O)_\gamma(NH_3)$) into a reactive (FastOM) and a refractory part (SlowOM), a list of chemical compounds to be represented in the model is first compiled: FastOM, SlowOM, DOC, O_2, Sal, CO_2, HCO_3^-, CO_3^{2-},

NH_3, NH_4^+, NO_3^-, SO_4^{2-}, HSO_4^-, H_2S, HS^-, $B(OH)_3$,

$B(OH)_4^-$, HF, F^-, OH^-, H^+

Note that "organic matter" ($(CH_2O)_\gamma(NH_3)$, FastOM, SlowOM) refers to particulate organic matter. Dissolved organic matter exhibits quasi conservative mixing in the Scheldt estuary (Soetaert et al., 2006) with a C/N ratio γ_{DOM} of 13.5 (average value for Scheldt estuary dissolved organic matter, T. van Engeland personal communication) and is conservatively modelled as [DOC]. Note that particulate matter is transported in the same manner as other dissolved state variables.

Taking into account air-sea exchange for CO_2, O_2, and NH_3 ($\mathbf{E}_{CO_2}$, $\mathbf{E}_{O_2}$, $\mathbf{E}_{NH_3}$) and advective-dispersive transport for all components ($\mathbf{Tr}_c$; c in {all participating species}), a mass balance for each chemical species in the model is created. Subsequently a series of linear combinations is performed to eliminate the equilibrium reaction terms from the mass balances. The resulting equations give implicit definitions for summed quantities which are invariant to equilibrium reactions (*equilibrium invariants*). These equilibrium invariants are equivalent to the mole balance equations for Morel's *components* of a system (Morel and Hering, 1993). For the model presented here, the linear combinations are chosen in such a way that the commonly used total concentration quantities $[\sum CO_2]$, $[\sum NH_4^+]$, $[\sum HSO_4^-]$, $[\sum H_2S]$, $[\sum BOH_3]$ and $[\sum HF]$ are obtained. Furthermore the mass balance equation for H^+ is linearly combined with the mass balances of other species in such a way that a subset of Dickson's total alkalinity [TA] (Dickson, 1981) is obtained as an equilibrium invariant. Note that for equilibrium invariants, all terms describing transport of individual species (e.g. for total alkalinity:

$\mathbf{Tr}_{HCO_3^-}$ +2 $\mathbf{Tr}_{CO_3^{2-}}$ +$\mathbf{Tr}_{B(OH)_4^-}$ ...) are lumped into one single term (e.g. for total alkalinity: $\mathbf{Tr}_{TA}$). This can be done since we assume that all substances are transported with the same tidal dispersion coefficient and our formulation of advective-dispersive transport is distributive over the sum under this assumption (this means there is no differential transport in our model).

Together with the concentrations of the species FastOM, SlowOM, DOC, O_2, NO_3^- and salinity (Sal), whose mass balance equations do not contain equilibrium terms (*kinetic species*), the given equilibrium invariants form a set of quantities independent of the chemical equilibrium reactions included in the model. Therefore, given suitable kinetic expressions for the modelled biogeochemical processes from Table 1, they can be numerically integrated. This feature allows using them as state variables of the model (Table 4, rates of change: Table 5).

2.2.5 pH

pH, or the free proton concentration $[H^+]$, is modelled since it can be used as a master variable to monitor the chemical state of a natural body of water, as almost any biogeochemical process occurring in such an environment affects $[H^+]$ either directly or indirectly (Stumm and Morgan, 1996; Soetaert et al., 2007). The free pH scale is used here, since all components of the systems in question are considered explicitly, including [HF] and $[HSO_4^-]$ (cf. Dickson, 1981).

Our model contains a pH calculation routine as given by Hofmann et al. (2007), which has been inspired by Luff et al. (2001) and Follows et al. (2006) (described in appendix A). Since pH data for the Scheldt estuary have been measured on the NBS pH scale (Durst, 1975), the modelled free scale pH was converted to the NBS scale using the activity coefficient for H^+, which is calculated by means of the Davies equation (Zeebe and Wolf-Gladrow, 2001). The use of the Davies equation is assumed to be a sufficient approximation, since according to Zeebe and Wolf-Gladrow (2001) it is valid up to ionic strengths of approximately 0.5 and yearly averaged salinity values at the mouth of the Scheldt estuary (the downstream boundary of our model) are about 28 resulting in

a ionic strength of approximately 0.57, while in the remaining estuary salinity values, hence ionic strengthes, are lower.

2.2.6 Data

All data that are referred to as *monitoring data* were obtained by the Netherlands Institute of Ecology (NIOO) for 16 stations in the Scheldt between Breskens/Vlissingen (The Netherlands) and Rupelmonde (Belgium) by monthly cruises of the NIOO RV "Luctor". River kilometres (distance from the start of the model domain at Rupelmonde) and locations of the stations can be found in Table 6, a map of the Scheldt estuary indicating the positions of the sampling stations is given in Fig. 1.

Calibration and validation data

Data for the state variables [$\sum NH_4^+$], [NO_3^-], [O_2], organic matter, pH (on the NBS scale) and salinity are available from the monitoring program. Data for 2003 have been used to calibrate the model and data for 2001, 2002, and 2004 have been used to independently validate it. The model does not distinguish between NO_3^- and NO_2^- and all data referring to the state variable [NO_3^-] are the summed values of [NO_3^-] plus [NO_2^-]. Data for organic matter (OM) have been calculated by assuming the measured percentage of nitrogen in the suspended particulate matter concentration to be available as particulate organic matter. Nitrification rates for the year 2003 were obtained from Andersson et al. (2006). They have been measured with the ^{15}N method at salinities 0, 2, 8, 18 and 28 in January, April, July and October 2003. Yearly averaged values of these rate measurements were used to independently validate the model, as these data have not been used in model development and calibration. Total alkalinity [TA] data for the year 2003 have been obtained from Frederic Gazeau (personal communication and Gazeau et al., 2005). These yearly averages are based on four to five measurements along the estuary from January to May 2003 and monthly measurements for all 16 Scheldt monitoring stations from June to December 2003. [$\sum CO_2$] data for 2003 have

been calculated from [TA] data, monitoring pH and salinity, temperature forcing data, and $[\sum B(OH)_3]$, and $[\sum NH_4^+]$ from the model.

Boundary condition forcings

Values measured at monitoring station WS1 are considered to be downstream boundary conditions and values of station WS16 to be upstream boundary conditions. For $[O_2]$, $[\sum NH_3]$, $[NO_3^-]$, [OM], [DOC] and salinity, monitoring data were used for upstream and downstream boundaries. Organic matter (OM) is partitioned in a reactive (FastOM) and a refractory (SlowOM) fraction. At the downstream boundary a fraction of 0.4 of the organic matter (Soetaert and Herman, 1995a) is considered FastOM, and for the upstream boundary a FastOM fraction of 0.6 has been derived by calibration. Boundary conditions for $[\sum CO_2]$ ($[\sum CO_2]$ upstream: 4700 mmol m^{-3}; downstream: 2600 mmol m^{-3}; constant for all modelled years) have been calibrated using data from the year 2003. For $[\sum HSO_4^-]$, $[\sum HF]$ and $[\sum B(OH)_3]$ they were calculated from salinity monitoring data using formulae given in appendix B3 (DOE, 1994). To ensure consistency, total alkalinity boundary concentrations were calculated from pH, salinity and temperature monitoring data and $[\sum CO_2]$ boundary conditions according to the total alkalinity definition used in our model (Dickson, 1981). The boundary concentrations for $[\sum H_2S]$ are assumed to be zero.

Physical condition forcings

Average daily wind speeds 10 m above the water are obtained from the website of the Royal Dutch Meteorological Institute (KNMI), station Vlissingen. However, Borges et al. (2004b) have shown that the mean wind values in the upstream region around Antwerp can be as low as 50% of the values at Vlissingen. The estuary is therefore divided into a wind sheltered riverine part and an exposed marine part more than x_d river kilometres away from the upstream boundary to the downstream boundary. In the sheltered riverine part, downscaled wind velocities are used to calculate air-water

exchange fluxes. We assume that the wind stays at a fraction $fr_w^{\mathrm{Min}}=0.75$ of the values at Vlissingen in the sheltered riverine part and sigmoidally rises to the values at Vlissingen in the exposed marine part according to the relation

$$V_w(x)=\left(fr_w^{\mathrm{Min}}+F(x)\cdot(1-fr_w^{\mathrm{Min}})\right)\cdot V_w(\mathrm{Vlissingen}) \tag{6a}$$

$$F(x)=\frac{(x-x_d)^2}{(x-x_{\max})^2+(x-x_d)^2} \tag{6b}$$

for every distance from the upstream boundary $x \geq x_d$, with $x_d=68.1$ km being the dividing distance between the wind exposed and the wind sheltered part of the estuary, $x_{\max}=104$ km being the length of the estuary, and V_w(Vlissingen) signifying the wind speed at Vlissingen. This expression is based on a generic dependency function given by Brinkman (1993).

River flows at the upstream boundary are obtained from the Ministry of the Flemish Community (MVG). Since the advective flow increases from the upstream boundary towards the north sea due to inputs by amongst others the Antwerp harbour and the channel Gent-Terneuzen (van Eck, 1999; Soetaert et al., 2006) and no downstream flow values for the modelled years were available, data from the years 1980 to 1988 obtained from the SAWES model (van Gils et al., 1993; Holland, 1991) have been used to calculate a flow profile along the estuary. This is done by calculating percentages of mean flow increase between SAWES model boxes from the 1980 to 1988 data and scaling the upstream-border data for the years 2001 to 2004 accordingly, implementing a total flow increase of around 45% from Rupelmonde to Vlissingen. This practice implies that the lateral input into a particular part of the estuary has the same concentration as the input from upstream of this area.

The average water depth D (Fig. 2) was obtained for 13 MOSES model boxes from Soetaert and Herman (1995b) and interpolated to centres and boundaries of the 100 model boxes used in this work. The cross sectional area A, has been obtained as a continuous function of river kilometres from Soetaert et al. (2006). Temperatures of the

water column are monthly monitoring data and range from around freezing in winter to roughly 25°C in summer. Along the estuary there is a small spatial gradient in yearly temperature averages from around 13°C close to Rupelmonde to 12°C at Vlissingen. At 40 km from Rupelmonde, roughly at the position of the entrance to the harbour of Antwerp (Zandvliet lock) the yearly temperature averages show a pronounced maximum around 1°C higher than values at the upstream boundary. This is probably due to a combined warming effect of the Antwerp harbour and the nuclear power plant at Doel roughly 4 km upstream of the temperature maximum. Tidal current velocities used to calculate piston velocity K_L are averages of the years 1997 to 2001 for the stations Vlissingen, Hansweert and Antwerp, taken from Borges et al. (2004b) and interpolated to the centre of each box.

2.3 Implementation and calibration

The spatial dimension of the model area along the estuary from Rupelmonde to Vlissingen is discretised by means of 100 supposedly homogeneous model boxes of 1.04 km length. These model boxes are assumed to have a tidally averaged volume (constant over time) and are numbered from i=1 (upstream) to i=100 (downstream).

The model has been implemented in FORTRAN using the modelling environment FEMME[3] (Soetaert et al., 2002) and numerically integrated over time with an Euler scheme using a time-step of 0.00781 days. Seasonal dynamics for the four model years were resolved but only yearly averages will be presented. Most post-processing of model output and creation of figures has been done with the R statistical computing environment (R Development Core Team, 2005).

Boundary and physical conditions (weather) are forced onto the model with monthly (wind-speed: daily) data from the respective years as described in Sect. 2.2.6.

An artificial spin-up year has been created, starting with arbitrary initial conditions

[3]The model code can be obtained from the corresponding author or from the FEMME website:http://www.nioo.knaw.nl/ceme/femme/

for all state variables and containing only the initial values for the year 2001 for each forcing function. After running this spin-up year to create suitable initial conditions, the years 2001 to 2004 were run consecutively using forcing data from the respective year. Since FEMME requires a value for each forcing function at the beginning and at the end of each year, data for the first and the last day of each year were calculated by interpolation. For these calculations also data from 2000 and 2005 were used.

During the model fitting procedure, 11 parameters were calibrated: 5 biochemical parameters, 3 boundary condition parameters, and 3 transport parameters. The transport formulation (parameters E_{max} and E_{Min}, see below) has been calibrated by comparing the model output to field data for Sal. [$\sum CO_2$] boundary conditions were calibrated by comparing the model output to [TA] data for 2003, and the parameters r^{Min}_{FastOM}, r^{Nit}, p, k_S^{Inh}, o^{Nit} as well as the fraction of OM that is considered FastOM at the upstream boundary were calibrated by comparing the model output to field data for [OM], [$\sum NH_4^+$], [NO_3^-], [O_2], and pH from the year 2003. The scale factor for the gas-exchange piston velocities s_{pist} was calibrated by comparing the model to data for pH and [O_2] from the year 2003.

3 Results

3.1 A relation between mean water depth D and tidal dispersion coefficients E

Following the idea put forward by Monismith et al. (2002) that there is proportionality between tidal dispersion and water depth and by comparing model output to field data for the conservative tracer salinity (see Fig. 3), we devised a linear relationship between tidal dispersion coefficients $E_{i-1,i}$ and mean water depth D_i for model box i:

$$E_{i-1,i} = E_{max} + (E_{max} - E_{Min}) \cdot \frac{D_i - D_{max}}{D_{max} - D_{Min}} \quad (7)$$

with

BGD
5, 83–161, 2008

E_{max}	350	$m^2 s^{-1}$
E_{Min}	70	$m^2 s^{-1}$
D_{max}	13.7	m
D_{Min}	6.0	m

Values for E_{max} and E_{Min} were calibrated (within the range of E values given in Soetaert and Herman, 1995b), while values for D_{max} and D_{Min} were obtained for the 13 MOSES model boxes from Soetaert and Herman (1995b).

While transport coefficients were calibrated for the year 2003, yearly averaged longitudinal salinity profiles could be reproduced for the years 2001, 2002, and 2004 (see Fig. 3) by imposing respective advective flows Q and boundary conditions for salinity.

In all years, salinity more than linearly increases from around 1 upstream to values between 14 and 22 at km 60 and subsequently increases in linear fashion to values between 26 and 30 at the downstream boundary.

3.2 Comparison of yearly averaged longitudinal concentration and rate profiles to measured data

Several parameters have been manually calibrated to improve the fit of the biogeochemical model against field data from the year 2003 (Fig. 3). Yearly averaged values for data are time weighted averages. While biogeochemical model parameters (and transport coefficients) were fitted for 2003, the model predictions for 2001, 2002, and 2004 did not involve further calibration. Model fits to data from those years can thus be considered as model validation. It can be seen that the model reproduces the data reasonably well; not only for the calibration year 2003 but also for the validation years, with all years showing similar patterns. $[\sum NH_4^+]$ values are between 70 and 115 mmol m^{-3} upstream, falling almost linearly to values around 10 mmol m^{-3} at km 50 and staying around this value in the downstream stretches. Nitrate concentrations initially rise from concentrations approximately between 323 and 343 mmol m^{-3} to con-

centrations approximately between 332 and 355 mmol m^{-3} at km 16, subsequently fall more than linearly to values of 140 to 215 mmol m^{-3} at km 60, and then further decline quasi-linearly to values between around 60 and 77 mmol m^{-3} in the most downstream model box. Oxygen concentrations start off at values between 65 and 92 mmol m^{-3} upstream, stay constant or even decline between river kilometres 0 and 20, followed by a quasi linear increase to values of ≈270 mmol m^{-3} at river km 60, and staying in this realm until the downstream border. The sum of the concentrations of both fractions of particulate organic matter shows larger discrepancy between model and data. It declines over the stretch of the estuary from values of 40 to 55 mmol m^{-3} upstream down to values of approximately 10 mmol m^{-3} downstream. The pH shows a sigmoidal increase from values around 7.57 to 7.63 upstream to values between 8.06 and 8.12 in the downstream part of the estuary. In all years a slight dip in the order of 0.01 to 0.05 pH values can be observed between km 0 to 30 preceding the sigmoidal increase.

Figure 4 shows the fit of predicted [TA] and [$\sum CO_2$] against observed data for the year 2003 ([$\sum CO_2$] data calculated from [TA] data). Note that those data (from the year 2003) have been used to calibrate only the $\sum CO_2$ boundary conditions for all four years. Both [TA] and [$\sum CO_2$] decrease in a sigmoidal fashion from upstream to downstream, [TA] from around 4460 mmol m^{-3} to 2760 mmol m^{-3}, and [$\sum CO_2$] from 4690 mmol m^{-3} to 2600 mmol m^{-3}.

Figure 5 compares the modelled nitrification rate ($\mathbf{R}_{Nit}$) for the year 2003 with field data obtained in the same year by Andersson et al. (2006) with the ^{15}N method. This is an independent model validation as these data have not been used in any way for calibration. It shows excellent agreement between measured and modelled nitrification rates, with an approximately linear decline in nitrification from 13.3 mmol m^{-3} d^{-1} to 0.5 mmol m^{-3} d^{-1} from km 0 to km 50, followed by a gradual decline to 0.12 mmol m^{-3} d^{-1} in the most downstream model box.

3.3 Sources and sinks for $\sum NH_4^+$, $\sum CO_2$, O_2 and NO_3^- along the estuary

3.3.1 Volumetric budgets

Since the model reproduces the spatial patterns of yearly averaged concentrations of $\sum NH_4^+$, $\sum CO_2$, O_2 and NO_3^- well for each of the four years, model rates can be used to compile budgets for these quantities. Figures 6 and 7 show cumulative plots of volumetric budgets along the estuary averaged over the years 2001 to 2004. A common feature is the pronounced activity in the upper estuary, i.e. between river km 0 and 55. In this stretch of estuary, the absolute values of almost all rates decline in a quasi linear fashion to stay at low levels until the mouth of the estuary.

It can be seen that $[\sum NH_4^+]$ (Fig. 6a ; Table 7) is mainly the result of a balance between nitrification ($\mathbf{R}_{Nit}$) consuming $\sum NH_4^+$ at a rate of $\approx$4721 mmol-N m^{-3} y^{-1} (99% of total loss at this position) at the upstream border and $\approx$42 mmol-N m^{-3} y^{-1} (28% of total loss at this position) in the downstream region, and advective-dispersive transport ($\mathbf{Tr}_{\sum NH_4^+}$) which imports $\sum NH_4^+$ at an upstream rate of $\approx$3179 mmol-N m^{-3} y^{-1} (67% of total input) and $\approx$80 mmol-N m^{-3} y^{-1} (70% of total input) at river km 60. The remaining gap is filled by $\sum NH_4^+$ production of oxic mineralisation ($\mathbf{R}_{Ox}$) and denitrification ($\mathbf{R}_{Den}$). Oxic mineralisation produces $\approx$935 mmol m^{-3} of $\sum NH_4^+$ per year (20% of total input) in the upstream region and $\approx$32 mmol-N m^{-3} y^{-1} (28% of total input) $\sum NH_4^+$ at km 60, denitrification produces $\approx$587 mmol-N m^{-3} y^{-1} (12% of total input) in the upstream part of the estuary, and has very little influence on $[\sum NH_4^+]$ in the downstream area (2% of total input at km 60; 4% of total input at km 104). Oxic mineralisation rates reach slightly higher values ($\approx$138 mmol-N m^{-3} y^{-1}; 94% of total input) at the downstream boundary than around km 60. This enhanced oxic mineralisation is counteracted by an advective-dispersive export of $\approx$103 mmol-N m^{-3} y^{-1} (70% of total loss at this position). For $[\sum NH_4^+]$, both sulfate reduction ($\mathbf{R}_{SRed}$) and ammonia air-water exchange ($\mathbf{E}_{NH_3}$) are negligible along the whole estuary, with contributions of less than 2% of the total

input or total loss of $[\sum NH_4^+]$ at all positions in the estuary.

The budget for $[\sum CO_2]$ (Fig. 6b; Table 8) is characterised by CO_2 loss to the atmosphere via air-water exchange ($\mathbf{E}_{CO_2}$), advective-dispersive $\sum CO_2$ input ($\mathbf{Tr}_{\sum CO_2}$), as well as $\sum CO_2$ production by oxic mineralisation ($\mathbf{R}_{OxCarb}$) and denitrification ($\mathbf{R}_{DenCarb}$). In the upstream regions around 7809 mmol-C m^{-3} y^{-1} (100% of total loss at this position) is lost to the atmosphere, while the rate decreases in the direction of the river flow, levelling off at values around 655 to 338 mmol-C m^{-3} y^{-1} (100% to 55% of total loss at this position) from km 60 to the downstream border. Oxic mineralisation produces ≈3808 mmol-C m^{-3} y^{-1} (49% of total input) at the upstream boundary, decreasing to ≈165 mmol-C m^{-3} y^{-1} (34% of total input) at km 60. $\sum CO_2$ production by denitrification decreases from ≈2391 mmol-C m^{-3} y^{-1} (31% of total input) at the upstream boundary to 25 mmol-C m^{-3} y^{-1} (4% of total input) at the downstream boundary. This value is not exceeded from km 56 onwards (values for km 56 not shown). Advective-dispersive $\sum CO_2$ import rises from ≈2031 mmol-C m^{-3} y^{-1} (24% of total input) at the upstream boundary to ≈4319 mmol-C m^{-3} y^{-1} (69% of total input) at km 22 to drop to levels below ≈550 mmol-C m^{-3} y^{-1} from km 50 onwards (values for km 50 not shown). Sulfate reduction ($\mathbf{R}_{SRed}$) accounts for 125 mmol-C m^{-3} y^{-1} (2% of total input) at the upstream boundary, is negligible in the mid part of the estuary due to low organic matter concentrations and therefore low total mineralisation, and accounts with 12 mmol-C m^{-3} y^{-1} again for 2% of the total $\sum CO_2$ production at the downstream boundary as dispersive import of reactive organic matter from the North Sea increases total mineralisation. As seen in the $[\sum NH_4^+]$ budget, oxic mineralisation rates increase again in the most downstream area, producing ≈574 mmol-C m^{-3} y^{-1} (94% of total input) at the downstream boundary. This again is counteracted by advective-dispersive transport, first in form of a reduced input per model box, and from km 95 on (values for km 95 not shown) again an export, reaching ≈272 mmol-C m^{-3} y^{-1} (45% of total consumption) at the downstream boundary. While being approximately balanced at the upstream and downstream boundary, in the mid part of the estuary the total loss of $\sum CO_2$ exceeds the total input, up to roughly 30% at km 60. Indeed, $[\sum CO_2]$ shows a decrease in time

(see below).

The budget for [O_2] (Fig. 7a; Table 9) is clearly dominated by oxygen consumption due to nitrification (-2 $\mathbf{R}_{Nit}$) and oxic respiration (-$\mathbf{R}_{OxCarb}$). Nitrification consumes oxygen at a rate of 9443 mmol-O_2 m^{-3} y^{-1} (71% of total loss at this position) at the upstream boundary, diminishing to 242 mmol-O_2 m^{-3} y^{-1} (34% of total loss at this position) at km 60 and staying at levels below that until the downstream boundary. Oxygen consumption by oxic mineralisation decreases from 3808 mmol-O_2 m^{-3} y^{-1} (29% of total consumption) at km 0 to 165 mmol-O_2 m^{-3} y^{-1} (23% of total loss at this position) at km 60, and rises again to 573 mmol-O_2 m^{-3} y^{-1} (87% of total loss at this position) at the downstream boundary. The oxygen consumption by these two processes is mainly counteracted by re-aeration ($\mathbf{E}_{O_2}$) which imports oxygen into the estuary at a rate between 8767 and 7117 mmol-O_2 m^{-3} y^{-1} (66% and 100% of total input) between kilometres 0 and 18, declines to 739 mmol-O_2 m^{-3} y^{-1} (100% of total input) at km 60 and reaches 157 mmol-O_2 m^{-3} y^{-1} (25% of total input) at the downstream boundary. Advective-dispersive transport ($\mathbf{Tr}_{O_2}$) imports oxygen at 4424 mmol-O_2 m^{-3} y^{-1} (34% of total input) at the upstream boundary, almost vanishes at km 18, exports oxygen from the model boxes in the midstream region (1947 mmol-O_2 m^{-3} y^{-1}, 64% of total loss at km 48), and imports it again at km 104 at a rate of 482.7 mmol-O_2 m^{-3} y^{-1} (75% of total input). The influence of sulfate re-oxidation on the oxygen concentration (-2 $\mathbf{R}_{SOx}$) can be neglected along the whole estuary.

[NO_3^-] along the estuary (Fig. 7a; Table 10) is governed by nitrate production due to nitrification ($\mathbf{R}_{Nit}$) and nitrate consumption due to denitrification (–0.8 $\mathbf{R}_{DenCarb}$) and advective-dispersive transport ($\mathbf{Tr}_{NO_3^-}$). Nitrification, the only nitrate producing process along the estuary, produces nitrate at 4721 mmol-N m^{-3} y^{-1} at the upstream boundary, declines to 121 mmol-N m^{-3} y^{-1} at km 60, and stays below this value in the rest of the estuary. Nitrate consumption of denitrification starts off at 1913 mmol-N m^{-3} y^{-1} (41% of total loss at this position) at the upstream boundary, goes down to 9 mmol-N m^{-3} y^{-1} (4% of total loss at this position) at km 60, and increases back to 20 mmol-

$N\,m^{-3}\,y^{-1}$ (28% of total loss at this position) at the downstream boundary. The influence of advective-dispersive transport diminishes from an export of 2783 mmol-N $m^{-3}\,y^{-1}$ (59% of total loss at this position) at the upstream boundary, to 194 mmol-N $m^{-3}\,y^{-1}$ (96% of total loss at this position) at km 60 and 52 mmol-N $m^{-3}\,y^{-1}$ (72% of total loss at this position) at km 104. At kilometres 60 and 104 an imbalance of total input and total loss of NO_3^- in favour of consumption can be noticed.

3.3.2 Volume integrated budgets

As the estuarine cross section area increases from 4000 m^2 upstream to around 76 000 m^2 downstream, there is a much larger estuarine volume in downstream model boxes than in upstream model boxes. Thus, volume integrated production or consumption rates (rates "per river km") are similar in the upstream and the downstream part of the estuary (in accordance with findings of Vanderborght et al., 2002), unlike in the volumetric plots, where the upstream region was clearly dominant. Figures 8 and 9 show volume integrated budgets along the estuary averaged for the years 2001 to 2004.

While for $\sum NH_4^+$ (Fig. 8a) the upstream and downstream regions are identified as most important in terms of total turnover, for $\sum CO_2$ (Fig. 8b) and O_2 (Fig. 9a) a pronounced maximum of total turnover can be distinguished at around km 50, identifying the area around the intertidal flat system of Saeftinge as the most important area. For NO_3^- the upstream area is most important, similar to its volumetric budget.

Figure 8a and Table 11 in combination with the percentages given in Table 7 show that, in contrast to the volumetric budget, volume integrated $\sum NH_4^+$ production due to oxic mineralisation ($\mathbf{R}_{Ox}$) is maximal at the downstream border with ≈10.4 Mmol-N $km^{-1}\,y^{-1}$. All other processes still contribute most to $[\sum NH_4^+]$ at the upstream boundary, as in the volumetric plots. In the volume integrated plot, the negative values of $\mathbf{Tr}_{\sum NH_4^+}$ (≈−7.8 Mmol-N $km^{-1}\,y^{-1}$) at the downstream boundary can be seen more clearly. In general, the estuary can be divided into three parts, a region of high total $\sum NH_4^+$ turnover between kilometres 0 and around 50, followed by a stretch of com-

paratively low total $\sum NH_4^+$ turnover between kilometres 50 and approximately 90, and finally, between kilometres 90 and 104 another region with high total $\sum NH_4^+$ turnover.

The volume integrated budget for $\sum CO_2$ (Fig. 8b; Table 11 in combination with Table 8) shows a distinct maximum of total $\sum CO_2$ turnover at km 48 with a total $\sum CO_2$ production of 56.6 Mmol-C km^{-1} y^{-1} and a total $\sum CO_2$ consumption of 63.5 Mmol-C km^{-1} y^{-1}. This maximum is followed by a slight dip in total turnover at km 60 with 20.2 Mmol-C km^{-1} y^{-1} total $\sum CO_2$ production and 27.6 Mmol-C km^{-1} y^{-1} total $\sum CO_2$ consumption. Further downstream, total $\sum CO_2$ turnover rates reach values slightly higher than in the upstream area. Around the downstream boundary, $\sum CO_2$ production by oxic mineralisation has its maximum at $\approx$ 43.7 Mmol-C km^{-1} y^{-1} and advective-dispersive transport exports $\sum CO_2$ at 21.0 Mmol-C km^{-1} y^{-1}, while it imports $\sum CO_2$ into the model box in question in almost all other stretches. Especially at kilometres 48, 60, and 67 it can be seen that the volume integrated total loss of $\sum CO_2$ is higher than the total $\sum CO_2$ production.

The volume integrated budget for O_2 (Fig. 9a; Table 11 in combination with Table 9) shows the same process patterns and basic shape as the volume integrated budget for $\sum CO_2$, with a maximum of absolute values of total O_2 turnover at km 48 (70.1 Mmol-O_2 km^{-1} y^{-1} total input; 68.7 Mmol-O_2 km^{-1} y^{-1} total loss at this position) followed by a dip in absolute values of total O_2 turnover at km 60 (31.2 Mmol-O_2 km^{-1} y^{-1} total input; 30.2 Mmol-O_2 km^{-1} y^{-1} total loss).

Unlike for the other chemical species, the volume integrated budget for NH_3^- (Fig. 9b; Table 11 in combination with Table 10) shows distinct maxima in total turnover at the upstream boundary (18.9 Mmol-N km^{-1} y^{-1} total input; 18.8 Mmol-N km^{-1} y^{-1} total loss at this position) and decreases towards the downstream boundary with 3.2 Mmol-N km^{-1} y^{-1} of total input at this position and 5.5 Mmol-N km^{-1} y^{-1} of total consumption. However, the resulting trumpet-like shape is not as pronounced as for the volumetric budget for $[NO_3^-]$.

3.3.3 Estuarine budgets

Figures 10 and 11 show budgets of $\sum NH_4^+$, $\sum CO_2$, O_2, and NO_3^- production and consumption, integrated over the whole model area and one year (averaged over the four modelled years).

Figure 10a shows a budget of total stock of $\sum NH_4^+$. It becomes clear that nitrification is the most important process affecting the $\sum NH_4^+$ stock in the estuary with a total loss of 0.83 Gmol (98% of total loss; σ=0.248 Gmol)[4] per year in the whole model region. This $\sum NH_4^+$ consumption is counteracted by $\sum NH_4^+$ production/import due to mainly advective-dispersive transport (0.476 Gmol; 57% of total input; σ=0.217 Gmol) and oxic mineralisation (0.306 Gmol; 37% of total input; σ=0.045 Gmol). Denitrification plays a minor role producing 0.043 Gmol (5% of total input; σ=0.007) of $\sum NH_4^+$ per year. Sulfate reduction and NH_3 air-water exchange both induce $\sum NH_4^+$ turnover with absolute values below 0.02 Gmol (≈2% of total input/consumption at this position) per year. There is a net reduction of the $\sum NH_4^+$ stock of 0.013 Gmol per year from the modelled region.

The stock of $\sum CO_2$ (Fig. 10b) is prominently influenced by out-gassing of CO_2 to the atmosphere, which consumes 3.58 Gmol (100% of total loss; σ=1.021 Gmol) of $\sum CO_2$ per year. Advective-dispersive input and oxic mineralisation supply $\sum CO_2$ at values of 1.96 Gmol (56% of total input; σ=1.028 Gmol) and 1.35 Gmol (38% of total input; σ=0.192 Gmol) per year, respectively. Again, denitrification has a minor influence, producing 0.183 Gmol (5% of total input; σ=0.031 Gmol) of inorganic carbon per year and sulfate reduction again stays below 0.02 Gmol (0% of total input) inorganic carbon production per year. A net reduction of the $\sum CO_2$ stock in the estuary of of 0.069 Gmol per year can be observed. This is evidenced by a decreasing [$\sum CO_2$] (see discussion).

In our model, oxygen (Fig. 11a) is only net supplied to the estuary via re-aeration (4.04 Gmol per model area and year; σ=0.828 Gmol). All other modelled processes

[4]The standard deviation σ is obtained from the yearly averaged values from all four modelled years for each process.

BGD
5, 83–161, 2008

consume oxygen, advective-dispersive transport net exports 1.01 Gmol to the sea (25% of total loss; σ=0.343 Gmol), oxic mineralisation consumes 1.35 Gmol (34% of total loss; σ=0.192 Gmol), nitrification 1.66 Gmol (41% of total loss; σ=0.496 Gmol), and sulfate re-oxidation can be neglected. A net gain of O_2 of 0.01 Gmol per year can be observed.

Finally, nitrate (Fig. 11b) is produced by nitrification at 0.83 Gmol (100% of total input; σ=0.248 Gmol), exported by advective-dispersive transport at 0.794 Gmol (84% of total loss; σ=0.353 Gmol), and consumed by denitrification at 0.147 Gmol (16% of total loss; σ=0.025 Gmol) per year, which means advective-dispersive export is around five times more important than denitrification in consuming the nitrate produced by nitrification. A net loss of nitrate of 0.111 Gmol per year can be noted.

3.4 Interannual differences

Although the freshwater discharge Q of the Scheldt shows no consistent trend during the years 1990 to 2004, it peaked in 2001 and fell rapidly until 2004 (Meire et al., 2005; Van Damme et al., 2005; van Eck, 1999), resulting in a downwards trend during our model time period. The plots in Fig. reffig: trends show trends of freshwater discharge Q, volume averaged Sal and $[CO_2]$, and CO_2 outgassing $\mathbf{E}_{CO_2}$ in the estuary from the year 2001 to 2004.

This decrease in Q is most likely the reason for several observed trends in our model, e.g. salinity Sal increases from 2001 to 2004 which is clearly a result of lowered freshwater discharge, as more saline seawater can enter the estuary (Meire et al., 2005; Van Damme et al., 2005). Similarly, the observed decrease in $[\sum CO_2]$ can be explained by less $\sum CO_2$ being imported into the estuary from the river at lower freshwater discharge ($[\sum CO_2]$ not shown). A decrease in $[\sum CO_2]$ also means a decrease in $[CO_2]$. However, via its influence on the dissociation constants K^*, salinity also influences $[CO_2]$, higher salinity meaning lower $[CO_2]$, reinforcing its downward trend from 2001 to 2004. Decreasing levels of $[CO_2]$ lower the CO_2 saturation state of the water and eventually lead to less CO_2 export to the atmosphere (The total amount of

CO_2 export to the atmosphere and the volume averaged saturation states for the four modelled years and the whole estuary are given in Table 12). Model runs with scaled freshwater flow (results not shown) confirm the inverse correlation between freshwater flow Q and $\mathbf{E}_{CO_2}$.

Furthermore, pH influences $[CO_2]$, higher pH implying lower $[CO_2]$. There was an upward trend in pH during our model years, which reinforces the downward trend in CO_2 export to the atmosphere. We believe that there is a relation between the decrease in freshwater flow and the upward trend in pH from 2001 to 2004, however, the exact mechanism for this relationship is not straight-forward. A mechanistic model able to quantify the influence of different modelled kinetic processes on the pH (Hofmann et al., 2007) will shed some further light on this issue.

4 Discussion

4.1 Model performance: data-model validation

Our objective was to construct a simple model reproducing observed data and interannual differences, allowing the establishment of annual budgets. Advective-dispersive transport is accurately reproduced (confer the fit of yearly averaged logitudinal profiles of the conservative tracer salinity, Fig. 3).

The model also reproduces $[\sum NH_4^+]$, $[NO_3^-]$, $[O_2]$, and pH versus river kilometres very well.

This level of performance has been achieved by using 7 biochemical parameters from literature and calibrating the other 5 using data for the year 2003. To run the model for the years 2001, 2002, and 2004, the upstream advective forcing, the temperature forcing, and the boundary concentrations have been adapted, but no further calibration was involved, making the fits for those years a model validation. Furthermore the model has been independently validated by comparing nitrification rates to field data from the year 2003 (Andersson et al., 2006) realising the objective of creating a tool

to examine interannual differences and annual budgets of key chemical species in the Scheldt estuary.

The very good overall performance of our rather simple model confirms the notion of Arndt et al. (2007) that for estuaries biogeochemical model complexity can be kept low as long as physical processes (i.e. advective-dispersive transport) are sufficiently resolved.

However, some features of the fits of state variables given in Fig. 3 suggest that the inclusion of processes transferring chemical species to algal and microbial biomass and back might make the model even more accurate. Modelled $[\sum NH_4^+]$ for example is slightly too high between river km 30 and km 50, which could be explained by microbial ammonium uptake (cf. Middelburg and Nieuwenhuize, 2000) and subsequent die off and agglomeration of microbes, explaining the measured organic matter concentrations that are slightly higher than the modelled ones in the downstream area. Furthermore oxygen values are slightly underestimated by the model in the region between km 30 and km 50. Together with pH values which are also slightly underestimated by the model in the same region, this could be explained by primary production which would rise the pH and produce oxygen. Between river km 35 and 50 the extended intertidal flat areas near Saeftinge are situated. A higher surface to volume ratio of the Scheldt water body in this area could enhance the effect of pelagic primary production (as well as benthic primary production due to a higher benthic-pelagic interface to volume ratio), however, this area also coincides with the location of the maximum turbidity zone in the Scheldt in medium dry periods (Meire et al., 2005) which implies bad light conditions for primary producers. And indeed Soetaert and Herman (1995c) report the highest degree of heterotrophy in the estuary around the turbidity maximum. Another reason for an underestimated organic matter concentration around the intertidal flat area of Saeftinge might be the fact that the model does not include any explicit organic matter input from this ecosystem consisting mainly of vascular plants. Although these and other arguments can be made about details, we consider the fit of our model good enough for our purposes.

4.1.1 Denitrification

Denitrification is not strongly constrained in our model because there are no data to constrain its rate.

Figure 13 shows the model fit for $[NO_3^-]$ with three different parametrisations for denitrification: our parametrisation based on literature values (solid black line), no denitrification (dashed red line) and denitrification maximised (dotted blue line) by using a very small $k_{NO_3^-}$ (10^{-8} mmol N m^{-3}) and a very large $k_{O_2}^{Inh}$ (10^8 mmol N m^{-3}), resulting in $\approx$0.6 Gmol NO_3^- consumption due to denitrification per year (compared to 0.2 Gmol y^{-1} with our parametrisation). Although the effect of denitrification on $[NO_3^-]$ along the estuary is small, this plot shows that our parametrisation based on literature values gives the best model performance.

Andersson (2007) reports 16 mmol m^{-2} d^{-1} of NO_3^- consumption due to denitrification for sediment from one lower estuary location in the Scheldt. Considering 338 km^2 of estuarine surface area, our model result of 0.2 Gmol NO_3^- consumption due to denitrification per year implies an average denitrification of 1.6 mmol NO_3^- m^{-2} d^{-1}, i.e. only one thenth of this number. Even with maximal denitrification and the associated worse model performance (Fig. 13), only a denitrification of 4.9 mmol NO_3^- m^{-2} d^{-1} can be achieved. This difference between our top-down whole estuarine estimate and the estimate of Andersson (2007) clearly shows the difficulties one encounters when upscaling sedimentary biogeochemical process rates over large areas and long timescales.

4.1.2 Air-water exchange: piston velocities

The fits of $[\sum CO_2]$, pH and $[O_2]$ show that air-sea exchanges for O_2 and CO_2 sufficiently represent reality. Although being specifically devised Raymond and Cole (2001) also state that piston velocities given in Borges et al. (2004b) and applied in Borges et al. (2004a) were not suitable for our model in their original form. Piston velocities calculated with our data according to Borges et al. (2004b) yield k_{600} values of $\approx$13 cm h^{-1}

(Fig. 14). These values are rather high, resulting in a poor fit for the yearly averaged pH in our model as the pH is too high along the whole estuary (Fig. 14). Raymond and Cole (2001) state that k_{600} in estuaries should be between 3 and 7 cm h^{-1} (Hellings et al. (2001) use values of 0.4 to 4.7 cm h^{-1}, Frankignoulle et al. (1998) use 8 cm h^{-1}, and Frankignoulle et al. (1996) suggest 8.4±3.1 cm h^{-1} for the Scheldt estuary) and that piston velocities obtained with floating chamber gas flux measurements, as done by Frankignoulle et al. (1998) and Borges et al. (2004b), tend to overestimate when applied over longer periods of time and for large areas. Furthermore wind speed values measured aboard a ship, as done by Borges et al. (2004b), are considered to be less reliable than wind from fixed weather stations as, e.g., the data we use. Several other wind dependent formulations for piston velocities were implemented: Banks and Herrera (1977); Wanninkhof (1992); Raymond and Cole (2001); McGillis et al. (2001); Clark et al. (1995); Liss and Merlivat (1986); Kuss et al. (2004); Nightingale et al. (2000). Of these formulations only the formulations of Kremer et al. (2003), Liss and Merlivat (1986), and McGillis et al. (2001) yield values which are in the appropriate range for our model as they produce a reasonable fit for pH in the downstream region of the estuary (Fig. 14). However, in the upstream stretches the pH is underestimated with these formulations, as the CO_2 export to the atmosphere is too low in that area. All other formulations mentioned above, except for Borges et al. (2004b), result in values which are too high for the model, and if scaled down result in a similar fit of pH (good in the downstream region, bad in the upstream region) as the formulations by Kremer et al. (2003) and Liss and Merlivat (1986). Although being inappropriately high in their original form, only the piston velocities obtained with the formulation of Borges et al. (2004b) scaled by a factor s_{pist}=0.25 result in a reasonably good fit for pH in both the upstream and the downstream region (however, the downstream pH fit is a bit worse than with the Kremer et al. (2003), Liss and Merlivat (1986), and McGillis et al. (2001) formulations). The piston velocity formulation provided by Borges et al. (2004b) is thus a function with an apt shape for the Scheldt estuary, which is most likely due to the fact that these authors explicitly include the effect of estuarine tidal current velocities in their

piston velocity formulation. Especially in the upstream regions of the Scheldt estuary, where the channel narrows and tidal current velocities increase, this effect seems to be significant. However, even using the scaled Borges et al. (2004b) piston velocities the fit for pH still could be improved. A higher spatial resolution in wind speed from fixed weather stations and a higher spatial and temporal resolution in tidal current velocity data would therefore be useful to obtain a better piston velocity formulation and thus more reliable estimates for CO_2 air water exchange. For future studies it might even turn out to be necessary to use different piston velocity formulations for the narrow upper part and the broad lower part of the Scheldt estuary. This is backed by the fact that also the pH simulations of Vanderborght et al. (2002), which use a single piston velocity formulation including tidal current velocity effects, perform differently in the upstream and downstream regions of the Scheldt estuary.

4.2 Volumetric budgets for $[\sum NH_4^+]$, $[\sum CO_2]$, $[O_2]$ and $[NO_3^-]$ (Figs. 6 and 7)

According to the volumetric budgets for $[\sum NH_4^+]$, $[\sum CO_2]$, $[O_2]$ and $[NO_3^-]$, the estuary can be divided into two parts, an upstream region (river km 0 until roughly km 55 at Walsoorden) and a downstream area, with process rates being up to an order of magnitude higher in the upstream part. This division, which is in accordance to findings of Vanderborght et al. (2007), Regnier et al. (1997), and Soetaert and Herman (1995a,c), is more pronounced for $[NO_3^-]$ and $[\sum NH_4^+]$ than for $[O_2]$ and $[\sum CO_2]$, because the latter two quantities also depend on gas exchange with the atmosphere which in turn only depends on the concentration of the species to be exchanged and not on the concentrations of other species. Biogeochemical rates, in contrast, usually depend on the concentrations of several substances. Therefore the rates of gas exchange processes decrease less than biogeochemical rates as nutrient levels decrease when going from upstream to downstream in the Scheldt estuary. However, $\mathbf{E}_{CO_2}$ is also strongly influenced by the pH in the estuary, which rises from ≈7.5 in the upstream regions to ≈8.1 downstream. This is because $\mathbf{E}_{CO_2}$ depends linearly on $[CO_2]$ which in turn depends on pH. A rising pH induces a declining $[CO_2]$. Considering the estuarine averages of

$[\sum CO_2] \approx 3400\,mmol\,m^{-3}$, T≈13°C, and Sal≈10, $[CO_2]$ declines by a factor of about 4 from around $130\,mmol\,m^{-3}$ to around $30\,mmol\,m^{-3}$ if the pH rose from around 7.5 to 8.1. This means, that the increase in pH along the estuary contributes to the decline in the absolute values of $\mathbf{E}_{CO_2}$ from upstream to downstream.

While the volumetric budgets for $[\sum NH_4^+]$ (Fig. 6a) and $[NO_3^-]$ (Fig. 7b) show relatively smooth features, the volumetric budget for $[\sum CO_2]$ (Fig. 6b) exhibits a more spiked pattern. Its shape is a result of the dependency of $[\sum CO_2]$ on CO_2 air-water exchange ($\mathbf{E}_{CO_2}$) which in turn is influenced by the estuarine depth D. This fact makes estuarine depth patterns visible in the budget for $[\sum CO_2]$. To a lesser extent the same can be seen in the volumetric budget for $[O_2]$ (Fig. 7a), which in the upper reaches of the estuary, between river km 0 and about 18, smoothly follows the $[\sum NH_4^+]$ budget (dominated by nitrification), but in the downstream part of the estuary also shows estuarine depth patterns, attributable to its dependency on O_2 air-water exchange ($\mathbf{E}_{O_2}$).

4.3 Oxygen budget (Fig. 11a)

It is clear that oxygen consumption by nitrification and oxic mineralisation, as well as by advective-dispersive export is balanced by oxygen import from the atmosphere. Similarly to Ouboter et al. (1998), in our model more than one third of the total oxygen consumption in the estuary is due to nitrification; oxygen consumption by oxic mineralisation is comparable to oxygen consumption by nitrification, similar to conditions reported by Regnier et al. (1997). To be noted, however, is that integrated over the whole estuary, nitrification consumes more oxygen per year than oxic mineralisation. In accordance with its heterotrophic nature (Gazeau et al., 2005), the estuary is a net consumer of oxygen, only about 34% of the oxygen entering the estuary by advection-dispersion and re-aeration leaves the estuary at the mouth. 88% of the total O_2 input into the estuary is due to re-aeration.

4.4 Synopsis of single species budgets: elemental budgets

Nitrogen and carbon budgets have been constructed for the entire estuary (Figs. 15 and 16). It can be seen that there is a net import of organic N and a net export of organic C at the downstream boundary. This is due to the different C/N ratios of fast and slow degrading organic matter: slow degrading OM with a high C/N ratio is mainly advected out, while a certain amount of fast degrading OM with a low C/N ratio is dispersed in.

4.4.1 Nitrogen (Fig. 15)

The Scheldt estuary is a net consumer of ammonium. The total advective-dispersive input at the upstream boundary per year ($(\mathbf{Tr}_{\sum NH_4^+})_{up}$), averaged over the years 2001 to 2004, of 0.58 Gmol $\sum NH_4^+$ is lower than the 0.83 Gmol $\sum NH_4^+$ consumed by nitrification per year in the same period. The sum of $\sum NH_4^+$ imports and production processes is 0.933 Gmol, 89% is consumed by nitrification within the estuary and roughly 11% leaves the estuary at the mouth. This number is comparable to the export of about 16% of the total input (including mineralisation processes) of $\sum NH_4^+$ in the years 1980 to 1986 as reported by Soetaert and Herman (1995a). However, the absolute values of process rates affecting $[\sum NH_4^+]$ in the years 2001 to 2004 are at about 20% of the values during the years 1980 to 1986. This is most likely due to reduced riverine nutrient and organic loadings and resulting lower $[\sum NH_4^+]$ in the years 2001 to 2004 as compared to 1980 to 1986 (Soetaert et al., 2006). Due to lower $[\sum NH_4^+]$ in 2001 to 2004, volumetric nitrification rates in the upstream region were 79%, at km 60 roughly 8%, and in the downstream region roughly 5% of the values in the early eighties as reported by Soetaert and Herman (1995a). Due to the large estuarine volume in the downstream region, the drop in nitrification in this area is mostly responsible for the drop in total ammonium consumption by nitrification in the whole estuary from the early eighties to our model time period (2001 to 2004).

This downward trend in total nitrification shows that the initial intensification of ni-

trification in the Scheldt due to increasing oxygen levels since the second half of the seventies (Van Damme et al., 2005; Soetaert and Herman, 1995c) has peaked and subsequently decreased again, most likely due to reduced ammonium concentrations in the estuary (Soetaert et al., 2006), suggesting a shift from initial oxygen limitation of nitrification towards ammonium limitation now. A similar shift as has happened in time can be observed longitudinally during our model time period, as nitrification is oxygen limited upstream and ammonium limited downstream. However, as in the seventies (Billen et al., 1985), eighties (Van Damme et al., 2005; Soetaert and Herman, 1995c; Regnier et al., 1997), and nineties (Vanderborght et al., 2007), nitrification remains the major process governing N cycling in this estuary.

Furthermore, the estuary is a net producer of nitrate in the year 2001 to 2004. Roughly 1.5 times as much nitrate leaves the estuary by advection-dispersion at the mouth of the estuary, as is advectively imported (confer Fig. 11b). Yet, the nitrate producing character of the Scheldt estuary diminished due to reduced nitrification rates from the early eighties until the beginning of the 21st century, as Soetaert and Herman (1995a) reported that three times as much nitrate was exported to the sea as entered the estuary in the eighties.

Only 8% of the total N input in the system (nitrate, ammonium and particulate and dissolved organic nitrogen together) is lost to the atmosphere as N_2 due to denitrification (Fig. 15), while the rest is exported to the Southern Bight of the North Sea. This shows a clear downwards trend in the percentage of N_2 production, as in the eighties 21–25% of the total nitrogen imported into the Scheldt (Soetaert and Herman, 1995a; Ouboter et al., 1998), and in the seventies around 40% (Soetaert and Herman, 1995a; Billen et al., 1985) of the total nitrogen import into the estuary was removed within the estuary, mainly due to denitrification. This phenomenon is likely due to improved oxygen conditions in the Scheldt from the seventies until now (Soetaert and Herman, 1995a; Soetaert et al., 2006), moving the zone of denitrification more into the narrow upstream regions and generally allowing for less and less denitrification because of the limited area of sediments, the prime location of denitrification. A downward trend in the

percentage of N_2 generated and escaping means an upward trend in the percentage of N export to the sea. In absolute values, however, this resulted initially in an increasing N export to the North Sea from the seventies to the eighties from 1.9 Gmol y^{-1} to 3.6 Gmol y^{-1} (Soetaert and Herman, 1995a), before it decreased to 2.3 Gmol y^{-1} in our model period. This decrease in N export is due to approximately halved input loads (4.7 Gmol y^{-1} in the eighties (Soetaert and Herman, 1995a), 2.4 Gmol y^{-1} in our model). Yet the N export to the sea in 2001 to 2004 is still higher than in the seventies, in spite of the fact that the input into the system was much higher then (3.7 Gmol y^{-1}, Billen et al., 1985). Table 13 summarises these numbers.

Note that these results should be considered tentative, since denitrification is poorly constrained in our model (Sect. 4.1.1).

4.4.2 Carbon (Fig. 16)

Estuaries are a significant source of CO_2 to the atmosphere and are even important on a global scale (Borges et al., 2006). Our model suggests an averaged CO_2 export to the atmosphere of 3.6 Gmol y^{-1}, which is about 14% of the total carbon input (including DOC) into the system (Fig. 16).

This value is much lower than values reported by others (Table 14). These discrepancies are most likely due to three reasons: 1) differences in the riverine discharge and resulting carbon import into the system (confer a factor 2 difference in $\mathbf{E}_{CO_2}$ from 2001 and 2004), 2) differences in estimates of the estuarine surface area which contributes to CO_2 air-sea exchange (see also Borges et al., 2006), and 3) an overestimation of the piston velocity parametrisation (Fig. 14) mostly due to overestimated gas exchange flux measurements with the floating chamber method (Raymond and Cole, 2001). This finding is in agreement with Vanderborght et al. (2002) who also reported modelled CO_2 air-water exchange values more than a factor 2 smaller than floating chamber flux measurements by Frankignoulle et al. (1998).

Considering that our estimate is based on a mechanistic model with rigorous mass conservation and yields a reasonable fit to the data only if downscaled piston velocities

are used, our results substantiate the suggestion of Borges et al. (2006) that the CO_2 export from the Scheldt estuary to the atmosphere given by Frankignoulle et al. (1998) is an overestimate. It also suggests that this is to a large extent due to an overestimate in the CO_2 flux values per m^2.

Frankignoulle et al. (1998) reported that in the Scheldt estuary two thirds of the CO_2 flux to the atmosphere results from heterotrophy and only one third from ventilation of riverine DIC and Abril et al. (2000) estimate that riverine DIC contributes only 10% to the total CO_2 outgassing of the Scheldt estuary. In contrast, our model suggests that, averaged over the four modelled years, 64% of the CO_2 export to the atmosphere can be attributed to ventilation of riverine DIC (based on results of model runs with and without biogeochemical processes).

5 Summary

The Scheldt estuary is an active biogeochemical reactor where, all along its path the transformations occur at a similar magnitude. This is due to the combined effects of very high volumetric process rates and small estuarine volume upstream, giving way to gradually decreasing volumetric rates and increasing estuarine volume downstream.

With respect to the nitrogen cycle, the estuary has evolved towards a more and more inert passage way of total nitrogen, with only 8% of the total imported nitrogen being lost from the estuary. This is in sharp contrast to the situation in the eighties and seventies where this loss amounted to more than 20% and 40%, respectively. Coinciding with a reduced total nitrogen import in the estuary, this has led to a current total nitrogen export to the North Sea which is smaller than the export in the eighties but still larger than what was observed in the seventies. However, the estuary has a large effect on the nitrogen speciation, especially by transforming ammonium and, indirectly, the imported organic nitrogen to nitrate. Similarly to previous budget estimates, nitrification remains the process consuming most of the oxygen within the estuary.

The loss of imported carbon in the estuary represents about 14%, and occurs

through physical ventilation of CO_2 to the atmosphere. Two thirds of this lost C is riverine-borne DIC, one third of the ventilated CO_2 originates from heterotrophic production in the estuary itself. Whilst the estuary remains a significant source of CO_2 to the atmosphere, our results suggest that previous literature estimates, based on upscaled in-situ field estimates may need downward revision.

Finally, in the four-year period (2001–2004) during which our model was applied, clear trends in the chemical concentrations and budgets were observed. These trends were clearly linked to the decreased freshwater discharge, that was halved in that period.

Appendix A

pH calculation

Hofmann et al. (2007) describe a step-by-step procedure of devising a pH model of an aquatic system. They mention different solution approaches, one of which is the improved operator splitting approach (OSA). This OSA is inspired by Luff et al. (2001) and Follows et al. (2006) and is implemented here.

In our model, total alkalinity is defined as $[TA]:=[HCO_3^-]+2\ [CO_3^{2-}]+[B(OH)_4^-]+[OH^-]+[HS^-]+[NH_3]-[H^+]-[HSO_4^-]-[HF]$. All components of this definition can be written as functions of $[H^+]$, the equilibrium invariants and the chemical equilibrium constants of the respective acid base system. For example $[HCO_3^-]$ can be expressed as:

$$[HCO_3^-]=\frac{K^*_{1CO_2}[H^+]}{[H^+]^2+K^*_{1CO_2}}[H^+]+K^*_{1CO_2}K^*_{2CO_2}[\sum CO_2] \quad \text{(A1)}$$

Using temperature and salinity dependent expressions for stoichiometric[5] dissociation

[5]Stoichiometric dissociation constants as opposed to thermodynamic dissociation con-

constants on the free-proton scale[6] ($K^*_{HSO_4^-}$: Dickson (1990b); K^*_{HF}: Dickson and Riley (1979); $K^*_{CO_2}$ and $K^*_{HCO_3^-}$: Roy et al. (1993); K^*_W: Millero (1995); $K^*_{B(OH)_3}$: Dickson (1990a); $K^*_{NH_4^+}$: Millero et al. (1995); $K^*_{H_2S}$: Millero et al. (1988)), pressure corrected according to Millero, 1995, [TA] can be expressed as functions of $[H^+]$, the equilibrium invariants and the involved dissociation constants K^*_x. Assuming constant conditions (state variables and K^*_x values constant) during a time-step of the numerical integration, the components of [TA] can be calculated as functions of $[H^+]$ only. This means that [TA] can be written as function of $[H^+]$ only:

$$TA([H^+]) = \frac{K^*_{CO_2}[H^+] + 2K^*_{CO_2}K^*_{HCO_3^-}}{[H^+]^2 + K^*_{CO_2}[H^+] + K^*_{CO_2}K^*_{HCO_3^-}}[\sum CO_2] + \ldots + \frac{K^*_W}{[H^+]} + \ldots - [H^+] - \ldots \quad \text{(A2)}$$

Given a consistent value for $[H^+]$, Eq. A2 should yield the same value for total alkalinity as the explicitly modelled total alkalinity (state variable) $[TA]_{mod}$. This allows to assess a consistent value for $[H^+]$ for every time-step and model box by finding the chemically meaningful root of the difference between the two quantities:

$$(TA([H^+]) - [TA]_{mod}) \stackrel{!}{=} 0 \quad \text{(A3)}$$

stants. For a discussion of different types of dissociation constants, see Zeebe and Wolf-Gladrow (2001)

[6]Since $[\sum HSO_4^-]$ and $[\sum HF]$ are modelled explicitly, all dissociation constants are used on the free pH scale (Dickson, 1984) and to be consistent with DOE (1994) concentration units of the dissociation constants are in kg of solution. Conversions to and from volumetric concentrations are done using the salinity and temperature dependent density of seawater formulation by Millero and Poisson (1981).

This can be done by numerical root finding, e.g. using the van Wijngaarden-Dekker-Brent (z-brent) or the Newton-Raphson method (Press et al., 1992).

However, according to Follows et al. (2006) the numerical effort can be reduced by using the fact that carbonate alkalinity ($[CA]:=[HCO_3^-]+2[CO_3^{2-}]$) makes up the biggest part of total alkalinity. This allows assuming that the contribution of the minor concentrations to total alkalinity ($[TA]^{minor}:=[B(OH)_4^-]+[OH^-]+[HS^-]+[NH_3]-[H^+]-[HSO_4^-]-[HF]=f([H^+])$) for the previous iteration step are the same as for the current iteration step. This means, [CA] for the current time-step can be estimated by

$$[CA]_{cur} \approx [TA]_{mod} - [TA]^{minor}_{prev} \tag{A4}$$

This allows us to calculate $[H^+]$ by iteratively solving the quadratic equation in $[H^+]$:

$$0=[CA]_{cur}\cdot[H^+]^2+\left(K^*_{CO_2}\cdot\left([CA]_{cur}-[\sum CO_2]\right)\right)\cdot[H^+]$$
$$+K^*_{CO_2}\cdot K^*_{HCO_3^-}\cdot\left([CA]_{cur}-2\cdot[\sum CO_2]\right) \tag{A5}$$

For our model this calculation requires about 1 to 2 iterations per model box and time-step to calculate $[H^+]$ with suitable accuracy, meaning that

$$\left(TA([H^+])-[TA]_{mod}\right)<\epsilon \tag{A6}$$

with $\epsilon=10^{-3}\,mmol\,m^{-3}$.

Appendix B

Functions of salinity and temperature

B1 Gas exchange constants ($f(T,\mathrm{Sal})$)

Empirical formulations for the temperature and salinity dependency of the gas exchange constants used here, can be brought into the generic form:

$$\ln \frac{K_X}{k_0^\circ} = A + \frac{B}{\frac{T}{K}} + C \ln\left(\frac{T}{K}\right) + D\frac{T}{K} + E\left(\frac{T}{K}\right)^2$$

$\frac{T}{K}$	=	temperature stripped of unit
A, B, C, D, E	=	$f(\mathrm{Sal})$
S	=	salinity
k_0°	=	unit of the constant

The coefficients for gas exchange constants (Henry's constants) for CO_2 and O_2:

$K_{0_{CO_2}}$ (Weiss, 1974)			$K_{0_{O_2}}$ derived from Weiss (1970)		
A	=	$0.023517\mathrm{Sal} - 167.81077$	A	=	$-846.9975 - 0.037362 \cdot \mathrm{Sal}$
B	=	9345.17	B	=	25559.07
C	=	23.3585	C	=	146.4813
D	=	$-2.3656\ 10^{-4}\ \mathrm{Sal}$	D	=	$-0.22204 + 0.00016504 \cdot \mathrm{Sal}$
E	=	$4.7036\ 10^{-7}\ \mathrm{Sal}$	E	=	$-2.0564 \cdot 10^{-7} \cdot \mathrm{Sal}$
k_0°	=	$\left[\mathrm{mol(kg-solnatm)^{-1}}\right]$	k_0°	=	$\left[\mu\mathrm{mol\,(kg-solnatm)^{-1}}\right]$

The formulation for $K_{0_{O_2}}$ has been derived using the formulation for a gravimetric $[O_2]_{sat}$ given in Weiss (1970). It has been converted from ml-O_2 (kg-soln)$^{-1}$ to μmol-

O_2 (kg-soln)$^{-1}$ using the molar volume of O_2 calculated with the virial equation using a first virial coefficient for oxygen at 273.0 K of $-22\,cm^3\,mol^{-1}$ (Atkins, 1996), a value of 8.314 Nm $(K \cdot mol)^{-1}$ for the gas constant R and an ambient pressure of 101 300 N m^{-2}. The expression for the Henry's constant has then been created by dividing the expression for the saturation concentration by an atmospheric oxygen fugacity of fO_2=0.20946 atm (Williams, 2004).

B2 Piston velocities ($f(T,\mathrm{Sal})$)

Note that for our model, the piston velocities given here are scaled by a factor of s_{pist}=0.25 to produce a reasonable fit of model and data.

$$K_{L_{CO_2}} = K_{L_{NH_3}} = k_{600_{CO_2}} \cdot \left(\frac{Sc_{CO_2}(T,Sal)}{600}\right)^{-\frac{1}{2}} \cdot 0.24$$

$$K_{L_{O_2}} = k_{530_{O_2}} \cdot \left(\frac{Sc_{O_2}(T,Sal)}{530}\right)^{-\frac{1}{2}} \cdot 0.24$$

$$k_{600_{CO_2}} = k_{530_{O_2}} = 1.0 + 1.719 \cdot (V_{curr})^{\frac{1}{2}} \cdot D^{-\frac{1}{2}} + 2.58 \cdot V_{wind}$$

$$Sc_{CO_2}(T,Sal) = \frac{Sc_{CO_2}(T,35) - Sc_{CO_2}(T,0)}{35} \cdot Sal + Sc_{CO_2}(T,0)$$

$$Sc_{CO_2}(T,35) = 2073.1 - 125.62\,T + 3.6276\,T^2 - 0.043219\,T^3$$

$$Sc_{CO_2}(T,0) = 1911.1 - 118.11\,T + 3.4527\,T^2 - 0.041320\,T^3$$

$$Sc_{CO_2}(T,Sal) = \frac{Sc_{O_2}(T,35) - Sc_{O_2}(T,0)}{35} \cdot Sal + Sc_{O_2}(T,0)$$

$$Sc_{CO_2}(T,35) = 1953.4 - 128.0\,T + 3.9918\,T^2 - 0.050091\,T^3$$

$$Sc_{O_2}(T,0) = 1800.6 - 120.10\,T + 3.7818\,T^2 - 0.047608\,T^3$$

V_{wind} = wind velocity 10 m above the water in m s^{-1}
V_{curr} = estuarine tidal current velocity cm s^{-1}
D = mean water depth in m.

B3 Total concentrations of seawater components (f(Sal))

In DOE (1994) a table of concentrations of seawater components relative to chlorinity is given that allows to infer formulations for total concentrations of all seawater components. The generic formula is:

F_X	=	$\frac{a_X}{MW_X} Cl$	mol (kg-soln)$^{-1}$
a_X	=	relative concentration of X with respect to chlorinity	–
MW_X	=	molecular weight of X	g mol^{-1}
Cl	=	chlorinity	‰

The formulae for the concentrations needed here, rewritten as functions of salinity with Sal=1.80655 · Cl (DOE, 1994), are:

total sulfate	$[\sum \mathrm{HSO_4^-}]$	$S_T = \frac{0.1400}{96.062} \frac{\mathrm{Sal}}{1.80655}$
total fluoride	$[\sum \mathrm{HF}]$	$F_T = \frac{0.000067}{18.9984} \frac{\mathrm{Sal}}{1.80655}$
total borate	$[\sum \mathrm{BOH_3}]$	$B_T = \frac{0.000232}{10.811} \frac{\mathrm{Sal}}{1.80655}$

Acknowledgements. This research was supported by the EU (Carbo-Ocean, 511176-2) and the Netherlands Organisation for Scientific Research (833.02.2002). This is a publication of the NIOO-CEME (Netherlands Institute of Ecology – Centre for Estuarine and Marine Ecology), Yerseke.

References

Abril, G., Etcheber, H., Borges, A. V., and Frankignoulle, M.: Excess atmospheric carbon dioxide transported by rivers into the Scheldt estuary, Cr. Acad. Sci. II A, 330, 761–768, 2000. 119

Andersson, M. G. I.: Nitrogen cycling in a turbid, tidal estuary, Ph.D. thesis, Universiteit Utrecht, 2007. 112

Andersson, M. G. I., Brion, N., and Middelburg, J. J.: Comparison of nitrifier activity versus growth in the Scheldt estuary – a turbid, tidal estuary in northern Europe, Aquat. Microb. Ecol., 42, 149–158, 2006. 88, 96, 102, 110, 150

Arndt, S., Vanderborght, J. P., and Regnier, P.: Diatom growth response to physical forcing in a macrotidal estuary: Coupling hydrodynamics, sediment transport, and biogeochemistry, J. Geophys. Res., 112, C05045, doi:10.1029/2006JC003581, 2007. 88, 111

Atkins, P. W.: Physikalische Chemie, VCH Weinheim, 2nd Edition., 1996. 90, 124

Banks, R. B. and Herrera, F. F.: Effect of Wind and Rain on Surface Reaeration, J. Env. Eng. Div.-Asce, 103, 489–503, 1977. 91, 113, 159

Billen, G., Somville, M., Debecker, E., and Servais, P.: A Nitrogen Budget of the Scheldt Hydrographical Basin, Neth. J. Sea Res., 19, 223–230, 1985. 85, 86, 117, 118

Borges, A. V., Delille, B., Schiettecatte, L. S., Gazeau, F., Abril, G., and Frankignoulle, M.: Gas transfer velocities of CO_2 in three European estuaries (Randers Fjord, Scheldt, and Thames), Limnol. Oceanogr., 49, 1630–1641, 2004a. 112

Borges, A. V., Vanderborght, J. P., Schiettecatte, L. S., Gazeau, F., Ferron-Smith, S., Delille, B., and Frankignoulle, M.: Variability of the gas transfer velocity of CO_2 in a macrotidal estuary (the Scheldt), Estuaries, 27, 593–603, 2004b. 91, 92, 97, 99, 112, 113, 114, 159

Borges, A. V., Schiettecatte, L. S., Abril, G., Delille, B., and Gazeau, E.: Carbon dioxide in European coastal waters, Estuar. Coast. Shelf Sci., 70, 375–387, 2006. 84, 118, 119

Brinkman, A. G.: Biological processes in the EcoWasp ecosystem model, Tech. Rep. ISSN: 0928-6896, Institute for Forestry and Nature Research (IBN-DLO), Wageningen, The Netherlands Netherlands Institute for Sea Research (NIOZ), Texel, The Netherlands, 1993. 98

Canfield, D., Thamdrup, B., and Kristensen, E.: Aquatic Geomicrobiology, Elsevier Academic Press, Adv. Mar. Biol., 48, 2005. 88

Clark, J. F., Schlosser, P., Simpson, H. J., Stute, M., Wanninkhof, R., and Ho, D. T.: Relationship between Gas Transfer Velocities and Wind Speeds in The Tidal Hudson River Determined by the Dual Tracer Technique, in: Air-Water Gas Transfer, edited by Jaehne, B. and Monahan, E., 785–800, AEON Verlag, 1995. 91, 113, 159

Cloern, J. E.: Our evolving conceptual model of the coastal eutrophication problem, Mar. Ecol. Progr. Ser., 210, 223–253, 2001. 84

de Bie, M. J. M., Speksnijder, A. G. C. L., Kowalchuk, G. A., Schuurman, T., Zwart, G., Stephen,

J. R., Diekmann, O. E., and Laanbroek, H. J.: Shifts in the dominant populations of ammonia-oxidizing beta-subclass Proteobacteria along the eutrophic Schelde estuary, Aquat. Microb. Ecol., 23, 225–236, 2001. 89

Dickson, A. G.: An Exact Definition of Total Alkalinity and a Procedure for the Estimation of Alkalinity and Total Inorganic Carbon from Titration Data, Deep-Sea Res., 28, 609–623, 1981. 94, 95, 97

Dickson, A. G.: Ph Scales and Proton-Transfer Reactions in Saline Media Such as Sea-Water, Geochim. Cosmochim. Ac., 48, 2299–2308, 1984. 121

Dickson, A. G.: Thermodynamics of the Dissociation of Boric-Acid in Synthetic Seawater from 273.15-K to 318.15-K, Deep-Sea Res., 37, 755–766, 1990a. 121

Dickson, A. G.: Standard Potential of the Reaction - AgCl(S)+1/2h-2(G)=Ag(S)+HCl(Aq) and the Standard Acidity Constant of the Ion Hso4- in Synthetic Sea-Water from 273.15-K to 318.15-K, J. Chem. Thermodyn., 22, 113–127, 1990b. 121

Dickson, A. G. and Riley, J. P.: Estimation of Acid Dissociation-Constants in Seawater Media from Potentiometric Titrations with Strong Base .1. Ionic Product of Water – Kw, Mar. Chem., 7, 89–99, 1979. 121

DOE: Handbook of Methods for the Analysis of the Various Parameters of the Carbon Dioxide System in Sea Water, ORNL/CDIAC-74, 1994. 97, 121, 125

Durst, R.: Standard Reference Materials: Standardisation of pH Measurements, NBS Special Publications, 260-53, 1975. 95

Follows, M. J., Ito, T., and Dutkiewicz, S.: On the solution of the carbonate chemistry system in ocean biogeochemistry models, Ocean Model., 12, 290–301, 2006. 95, 120, 122

Frankignoulle, M., Bourge, I., and Wollast, R.: Atmospheric CO_2 Fluxes in a Highly Polluted Estuary (the Scheldt), Limnolo. Oceanogr., 41, 365–369, 1996. 113

Frankignoulle, M., Abril, G., Borges, A., Bourge, I., Canon, C., DeLille, B., Libert, E., and Theate, J. M.: Carbon dioxide emission from European estuaries, Science, 282, 434–436, 1998. 84, 86, 113, 118, 119, 145

Froelich, P. N., Klinkhammer, G. P., Bender, M. L., Luedtke, N. A., Heath, G. R., Cullen, D., Dauphin, P., Hammond, D., Hartman, B., and Maynard, V.: Early Oxidation of Organic-Matter in Pelagic Sediments of the Eastern Equatorial Atlantic - Suboxic Diagenesis, Geochim. Cosmochim. Ac., 43, 1075–1090, 1979. 88

Gazeau, F., Gattuso, J. P., Middelburg, J. J., Brion, N., Schiettecatte, L. S., Frankignoulle, M., and Borges, A. V.: Planktonic and whole system metabolism in a nutrient-rich estuary (the

Scheldt estuary), Estuaries, 28, 868–883, 2005. 86, 87, 96, 115, 145, 149
Gurney, W. S. C. and Nisbet, R. M.: Ecological Dynamics, Oxford University Press, 1998. 89
Heip, C.: Biota and Abiotic Environment in the Westerschelde Estuary, Hydrobiological Bulletin, 22, 31–34, 1988. 86
Helder, W. and Devries, R. T. P.: Estuarine Nitrite Maxima and Nitrifying Bacteria (Ems-Dollard Estuary), Neth. J. Sea Res., 17, 1–18, 1983. 89
Hellings, L., Dehairs, F., Van Damme, S., and Baeyens, W.: Dissolved inorganic carbon in a highly polluted estuary (the Scheldt), Limnol. Oceanogr., 46, 1406–1414, 2001. 86, 113, 145
Hofmann, A. F., Meysman, F. J. R., Soetaert, K., and Middelburg, J. J.: A step-by-step procedure for pH model construction in aquatic systems, Biogeosciences Discuss., 4, 3723–3798, 2007, http://www.biogeosciences-discuss.net/4/3723/2007/. 94, 95, 110, 120
Holland, A.: The waste loads on the Scheldt estuary (1980–1988), Tidal Waters Division, Middelburg, The Netherlands, 1991. 98
KNMI: Website of the Royal Dutch Meteorolgical Institute, http://www.knmi.nl/. 97
Kremer, J. N., Reischauer, A., and D'Avanzo, C.: Estuary-specific variation in the air-water gas exchange coefficient for oxygen, Estuaries, 26, 829–836, 2003. 91, 113, 159
Kuss, J., Nagel, K., and Schneider, B.: Evidence from the Baltic Sea for an enhanced CO_2 air-sea transfer velocity, Tellus B, 56, 175–182, 2004. 91, 113, 159
Liss, P. S. and Merlivat, L.: Air-Sea Gas Exchange Rates: Introduction and Synthesis, in: The Role of Air-Sea Exchange in Geochemical Cycling, edited by Buat-Menard, P., 113–127, D. Reidel Publishing Company, 1986. 91, 113, 159
Luff, R., Haeckel, M., and Wallmann, K.: Robust and fast FORTRAN and MATLAB (R) libraries to calculate pH distributions in marine systems, Comput. Geosci., 27, 157–169, 2001. 95, 120
McGillis, W. R., Edson, J. B., Hare, J. E., and Fairall, C. W.: Direct covariance air-sea CO_2 fluxes, J. Geophys. Res.-Oceans, 106, 16 729–16 745, 2001. 91, 113, 159
Meire, P., Ysebaert, T., Van Damme, S., Van den Bergh, E., Maris, T., and Struyf, E.: The Scheldt estuary: A description of a changing ecosystem, Hydrobiologia, 540, 1–11, 2005. 86, 87, 109, 111
Middelburg, J. J. and Nieuwenhuize, J.: Uptake of dissolved inorganic nitrogen in turbid, tidal estuaries, Mar. Ecol. Prog. Ser., 192, 79–88, 2000. 111
Millero, F. J.: Thermodynamics of the Carbon-Dioxide System in the Oceans, Geochim. Cos-

mochim. Ac., 59, 661–677, 1995. 121
Millero, F. J. and Poisson, A.: International One-Atmosphere Equation of State of Seawater, Deep-Sea Res., 28, 625–629, 1981. 91, 121
Millero, F. J., Plese, T., and Fernandez, M.: The Dissociation of Hydrogen-Sulfide in Seawater, Limnol. Oceanogr., 33, 269–274, 1988. 121
Millero, F. J., Yao, W. S., and Aicher, J.: The Speciation of Fe(II) and Fe(III) in Natural-Waters, Mar. Chem., 50, 21–39, 1995. 121
Monismith, S. G., Kimmerer, W., Burau, J. R., and Stacey, M. T.: Structure and flow-induced variability of the subtidal salinity field in northern San Francisco Bay, J. Phys. Oceanogr., 32, 3003–3019, 2002. 92, 100
Morel, F. M. and Hering, J. G.: Principles and Applications of Aquatic Chemistry, John Wiley & sons, 1993. 94
MVG: Ministerie van de Vlaamse Gemeenschap – Afdeling Maritieme toegang. 98
Nightingale, P. D., Liss, P. S., and Schlosser, P.: Measurements of air-sea gas transfer during an open ocean algal bloom., Geophys. Res. Lett., 27, 2117–2120, 2000. 91, 113, 159
Ouboter, M. R. L., Van Eck, B. T. M., Van Gils, J. A. G., Sweerts, J. P., and Villars, M. T.: Water quality modelling of the western Scheldt estuary, Hydrobiologia, 366, 129–142, 1998. 92, 115, 117
Peters, J. and Sterling, A.: L Estuaire de l Escaut, Project Mer, Rapport final, vol. 10, chap. Hydrodynamique et transports de sediments de l estuaire de l Escaut, 1–65, Service de Premier Ministre, Bruxelles, 1976. 87
Plambeck, J. A.: Introductory University Chemistry I - Solutions and Solubility, http://dwb.unl.edu/Teacher/NSF/C09/C09Links/www.chem.ualberta.ca/courses/plambeck/p101/p01182.htm, 1995. 91
Press, W., Teukolsky, S., and Vetterling, W.: Numerical recipes in FORTRAN : the art of scientific computing, Cambridge University Press, Cambridge, 2nd Ed., 1992. 122
R Development Core Team: R: A language and environment for statistical computing, R Foundation for Statistical Computing, Vienna, Austria,available at: http://www.R-project.org, ISBN 3-900051-07-0, 2005. 99
Raymond, P. A. and Cole, J. J.: Gas exchange in rivers and estuaries: Choosing a gas transfer velocity, Estuaries, 24, 312–317, 2001. 91, 112, 113, 118, 159
Regnier, P., Wollast, R., and Steefel, C. I.: Long-term fluxes of reactive species in macrotidal estuaries: Estimates from a fully transient, multicomponent reaction-transport model, Mar.

Chem., 58, 127–145, 1997. 85, 88, 89, 114, 115, 117
Roy, R. N., Roy, L. N., Vogel, K. M., PorterMoore, C., Pearson, T., Good, C. E., Millero, F. J., and Campbell, D. M.: The dissociation constants of carbonic acid in seawater at salinities 5 to 45 and temperatures O to 45 degrees C, Mar. Chem., 52, 183–183, 1993. 121
Sakurai, T., Fujita, S., Hayami, H., and Furuhashi, N.: A case study of high ammonia concentration in the nighttime by means of modeling analysis in the Kanto region of Japan, Atmos. Environ., 37, 4461–4465, 2003. 91
Soetaert, K. and Herman, P. M. J.: One Foot in the Grave - Zooplankton Drift into the Westerschelde Estuary (the Netherlands), Mar. Ecol. Prog. Ser., 105, 19–29, 1994. 85
Soetaert, K. and Herman, P. M. J.: Nitrogen Dynamics in the Westerschelde Estuary (Sw Netherlands) Estimated by Means of the Ecosystem Model Moses, Hydrobiologia, 311, 225–246, 1995a. 85, 86, 88, 89, 97, 114, 116, 117, 118
Soetaert, K. and Herman, P. M. J.: Estimating Estuarine Residence Times in the Westerschelde (the Netherlands) Using a Box Model with Fixed Dispersion Coefficients, Hydrobiologia, 311, 215–224, 1995b. 85, 87, 92, 98, 101
Soetaert, K. and Herman, P. M. J.: Carbon Flows in the Westerschelde Estuary (the Netherlands) Evaluated by Means of an Ecosystem Model (Moses), Hydrobiologia, 311, 247–266, 1995c. 85, 87, 111, 114, 117
Soetaert, K., Herman, P. M. J., and Middelburg, J. J.: A model of early diagenetic processes from the shelf to abyssal depths, Geochim. Cosmochim. Ac., 60, 1019–1040, 1996. 88, 89
Soetaert, K., deClippele, V., and Herman, P.: FEMME, a flexible environment for mathematically modelling the environment, Ecol. Model., 151, 177–193, 2002. 99
Soetaert, K., Middelburg, J. J., Heip, C., Meire, P., Van Damme, S., and Maris, T.: Long-term change in dissolved inorganic nutrients in the heterotropic Scheldt estuary (Belgium, The Netherlands), Limnol. Oceanogr., 51, 409–423, 2006. 84, 85, 86, 87, 94, 98, 116, 117
Soetaert, K., Hofmann, A. F., Middelburg, J. J., Meysman, F. J., and Greenwood, J.: The effect of biogeochemical processes on pH, Mar. Chem., 105, 30–51, 2007. 95
Stumm, W. and Morgan, J. J.: Aquatic Chemistry: Chemical Equilibria and Rates in natural Waters, Wiley Interscience, New York, 1996. 90, 95
Thomann, R. V. and Mueller, J. A.: Principles of Surface Water Quality Modeling and Control, Harper & Row, New York, 1987. 90, 92
Van Damme, S., Struyf, E., Maris, T., Ysebaert, T., Dehairs, F., Tackx, M., Heip, C., and Meire, P.: Spatial and temporal patterns of water quality along the estuarine salinity gradient of

the Scheldt estuary (Belgium and The Netherlands): results of an integrated monitoring approach, Hydrobiologia, 540, 29–45, 2005. 86, 87, 109, 117
van Eck, B.: De Scheldeatlas: een beeld van een estuarium, Schelde Informatie Centrum / Rijksinstituut voor Kust en Zee, Middelburg, 1999. 98, 109
van Gils, J. A. G., Ouboter, M. R. L., and De Roij, N. M.: Modelling of Water and Sediment Quality in the Scheldt Estuary, Netherlands J. Aquat. Ecol., 27, 257–265, 1993. 98
Vanderborght, J. P., Wollast, R., Loijens, M., and Regnier, P.: Application of a transport-reaction model to the estimation of biogas fluxes in the Scheldt estuary, Biogeochemistry, 59, 207–237, 2002. 86, 87, 106, 114, 118, 145
Vanderborght, J.-P., Folmer, I. M., Aguilera, D. R., Uhrenholdt, T., and Regnier, P.: Reactive-transport modelling of C, N, and O_2 in a river-estuarine-coastal zone system: Application to the Scheldt estuary, Marine Chemistry Special issue: Dedicated to the memory of Professor Roland Wollast, 106, 92–110, 2007. 85, 86, 87, 114, 117
Wanninkhof, R.: Relationship between Wind-Speed and Gas-Exchange over the Ocean, J. Geophys. Res.-Oceans, 97, 7373–7382, 1992. 91, 92, 113, 159
Weiss, R. F.: Solubility of Nitrogen, Oxygen and Argon in Water and Seawater, Deep-Sea Res., 17, 721–735, 1970. 91, 123
Weiss, R. F.: Carbon dioxide in water and seawater: the solubility of a non-ideal gas, Mar. Chem., 2, 203–215, 1974. 91, 123
Williams, D. R.: NASA Earth Fact Sheet, 2004. 91, 124
Zeebe, R. E. and Wolf-Gladrow, D.: CO_2 in Seawater: Equilibrium, Kinetics, Isotopes, no. 65 in Elsevier Oceanography Series, Elsevier, 1. Edition, 2001. 93, 95, 121

Table 1. Biogeochemical processes.

$\mathbf{R}_{Ox}$	:	$(CH_2O)_\gamma(NH_3)+\gamma O_2$	$\rightarrow$	$NH_3+\gamma CO_2+\gamma H_2O$
$\mathbf{R}_{Den}$	:	$(CH_2O)_\gamma(NH_3)+0.8\gamma NO_3\pm0.8\gamma H^+$	$\rightarrow$	$NH_3+\gamma CO_2+0.4\gamma N^{2+}1.4\gamma\ H_2O$
$\mathbf{R}_{SRed}$	:	$(CH_2O)_\gamma(NH_3)+\frac{\gamma}{2}SO_4^{2-}+\gamma H^+$	$\rightarrow$	$NH_3+\gamma CO_2+\frac{\gamma}{2}H_2S+\gamma H_2O$
$\mathbf{R}_{Nit}$	:	$NH_3+2\ O_2$	$\rightarrow$	$NO_3^-+H_2O+H^+$
$\mathbf{R}_{SOx}$	:	$H_2S+2\ O_2$	$\rightarrow$	$SO_4^{2-}+2\ H^+$

Table 2. Kinetic process formulation with 2 organic matter fractions (X in {FastOM, SlowOM }). Note that the notation [Z] signifies the concentration of species Z.

Oxic Mineralisation			
$\mathbf{R}_{OxX}$	=	$rt_X^{Min} \cdot OxLim \cdot [X]$	mmol N m^{-3} d^{-1}
$\mathbf{R}_{Ox}$	=	$\sum \mathbf{R}_{OxX}$	mmol N m^{-3} d^{-1}
$\mathbf{R}_{OxCarb}$	=	$\sum (\mathbf{R}_{OxX} \cdot \gamma_X)$	mmolC m^{-3} d^{-1}
Denitrification			
$\mathbf{R}_{DenX}$	=	$rt_X^{Min} \cdot DenLim \cdot [X]$	mmol N m^{-3} d^{-1}
$\mathbf{R}_{Den}$	=	$\sum \mathbf{R}_{DenX}$	mmol N m^{-3} d^{-1}
$\mathbf{R}_{DenCarb}$	=	$\sum (\mathbf{R}_{DenX} \cdot \gamma_X)$	mmol C m^{-3} d^{-1}
Sulfate Reduction			
$\mathbf{R}_{SRedX}$	=	$rt_X^{Min} \cdot SRedLim \cdot [X]$	mmol N m^{-3} d^{-1}
$\mathbf{R}_{SRed}$	=	$\sum \mathbf{R}_{SRedX}$	mmolN m^{-3} d^{-1}
$\mathbf{R}_{SRedCarb}$	=	$\sum (\mathbf{R}_{SRedX} \cdot \gamma_X)$	mmol C m^{-3} d^{-1}
Nitrification			
$\mathbf{R}_{Nit}$	=	$r^{Nit} \cdot f_{Q10} \cdot f_{O_2} \cdot f_{Sal}^{Inh} \cdot [\sum NH_3]$	mmol N m^{-3} d^{-1}
Sulfide Reoxidation			
$\mathbf{R}_{SOx}$	=	$r^{SOx} \cdot f_{Q10} \cdot f_{O_2} \cdot [\sum H_2S]$	mmol S m^{-3} d^{-1}
rt_X^{Min}	=	$r_X^{Min} \cdot f_{Q10}$	d^{-1}
f_{Q10}	=	$q10^{(T-q10_{t0})\cdot 10^{-1}}$	–
$f_{O_2}^{Inh}$	=	$k_{O_2}^{Inh} \cdot \left([O_2] + k_{O_2}^{Inh}\right)^{-1}$	–
f_{O_2}	=	$[O_2] \cdot \left([O_2] + k_{O_2}\right)^{-1}$	–
$f_{NO_3^-}^{Inh}$	=	$k_{NO_3^-}^{Inh} \cdot \left([NO_3^-] + k_{NO_3^-}^{Inh}\right)^{-1}$	–
$f_{NO_3^-}$	=	$[NO_3^-] \cdot \left([NO_3^-] + k_{NO_3^-}\right)^{-1}$	–
f_{Sal}^{Inh}	=	$o^{Nit} + (k_{Sal}^{Inh})^p \cdot \left((k_{Sal}^{Inh})^p + (Sal)^p\right)^{-1} \cdot (1 - o^{Nit})$	–
$\sum MinLim$	=	$f_{O_2} + f_{O_2}^{Inh} \cdot \left(f_{NO_3^-}^{Den} + f_{NO_3^-}^{Inh}\right)$	–
OxLim	=	$\sum MinLim^{-1} \cdot f_{O_2}$	–
DenLim	=	$\sum MinLim^{-1} \cdot f_{O_2}^{Inh} \cdot f_{NO_3^-}$	–
SRedLim	=	$\sum MinLim^{-1} \cdot f_{O_2}^{Inh} \cdot f_{NO_3^-}^{Inh}$	–
parameters			
$q10$	=	2.0	–
$q10_{t0}$	=	15.0	°C
$k_{O_2}^{Inh}$	=	22.0	mmol O_2 m^{-3}
k_{O_2}	=	30.0	mmol O_2 m^{-3}
$k_{NO_3^-}$	=	45.0	mmol N m^{-3}
$k_{NO_3^-}^{Inh}$	=	15.0	mmol N m^{-3}
r_{FastOM}^{Min}	=	0.15	d^{-1}
r_{SlowOM}^{Min}	=	0.002	d^{-1}
$r^{Nit} = r^{SOx}$	=	0.27	d^{-1}
p	=	3.0	–
k_{Sal}^{Inh}	=	4.0	–
o^{Nit}	=	0.05	–
γ_{FastOM}	=	4.0	mol C $(mol\,N)^{-1}$
γ_{SlowOM}	=	12.0	mol C $(mol\,N)^{-1}$

BGD
5, 83–161, 2008

EGU

Table 3. Left: Acid-base equilibria taken into account in the model. Right: Stoichiometric equilibrium constants.

$\mathbf{R}_a^{eq}$	:	CO_2+H_2O	$\rightleftharpoons$	$H^+ + HCO_3^-$	$K^*_{CO_2}$	=	$\frac{[H^+][HCO_3^-]}{[CO_2]}$
$\mathbf{R}_b^{eq}$	:	HCO_3^-	$\rightleftharpoons$	$H^+ + CO_3^{2-}$	$K^*_{HCO_3^-}$	=	$\frac{[H^+][CO_3^{2-}]}{[HCO_3^-]}$
$\mathbf{R}_c^{eq}$	:	H_2O	$\rightleftharpoons$	$H^+ + OH^-$	K^*_W	=	$[H^+][OH^-]$
$\mathbf{R}_d^{eq}$	:	$B(OH)_3+H_2O$	$\rightleftharpoons$	$H^+ + B(OH)_4^-$	$K^*_{B(OH)_3}$	=	$\frac{[H^+][B(OH)_4^-]}{[B(OH)_3]}$
$\mathbf{R}_e^{eq}$	:	NH_4^+	$\rightleftharpoons$	$H^+ + NH_3$	$K^*_{NH_4^+}$	=	$\frac{[H^+][NH_3]}{[NH_4^+]}$
$\mathbf{R}_f^{eq}$	:	HSO_4^-	$\rightleftharpoons$	$H^+ + SO_4^{2-}$	$K^*_{HSO_4^-}$	=	$\frac{[H^+][SO_4^{2-}]}{[HSO_4^-]}$
$\mathbf{R}_g^{eq}$	:	H_2S	$\rightleftharpoons$	$H^+ + HS^-$	$K^*_{H_2S}$	=	$\frac{[H^+][HS^-]}{[H_2S]}$
$\mathbf{R}_h^{eq}$	:	HF	$\rightleftharpoons$	$H^+ + F^-$	K^*_{HF}	=	$\frac{[H^+][F^-]}{[HF]}$

Table 4. State variables of the biogeochemical model.

kinetic species:			
[FastOM]	mmol N	m^{-3}	fast decaying particulate organic matter: $[(CH_2O)_{\gamma_{FastOM}}(NH_3)]$
[SlowOM]	mmol N	m^{-3}	slow decaying particulate organic matter: $[(CH_2O)_{\gamma_{SlowOM}}(NH_3)]$
[DOC]	mmol C	m^{-3}	conservative dissolved organic matter: $[(CH_2O)(NH_3)_{(\gamma_{SlowOM})^{-1}}]$
$[O_2]$	mmol O_2	m^{-3}	
$[NO_3^-]$	mmolN	m^{-3}	$[NO_3^-]+[NO_2^-]$
Sal	–		salinity
equilibrium invariants:			
$[\sum CO_2]$	mmolC	m^{-3}	$[CO_2]+[HCO_3^-]+[CO_3^{2-}]$
$[\sum NH_4^+]$	mmolN	m^{-3}	$[NH_3]+[NH_4^+]$
$[\sum HSO_4^-]$	mmolS	m^{-3}	$[HSO_4^-]+[SO_4^{2-}]$
$[\sum H_2S]$	mmolS	m^{-3}	$[H_2S]+[HS^-]$
$[\sum B(OH)_3]$	mmolB	m^{-3}	$[B(OH)_3]+[B(OH)_4^-]$
$[\sum HF]$	mmolF	m^{-3}	$[HF]+[F^-]$
[TA]	mmol	m^{-3}	$[HCO_3^-]+2[CO_3^{2-}]+[B(OH)_4^-]+[OH^-]+[HS^-]+[NH_3]-[H^+]-[HSO_4^-]-[HF]$

Table 5. Rates of change of model state variables (X in FastOM,SlowOM).

$$\frac{d[X]}{dt} = \mathbf{Tr}_X - \mathbf{R}_{OxX} - \mathbf{R}_{DenX} - \mathbf{R}_{SRedX}$$

$$\frac{d[DOC]}{dt} = \mathbf{Tr}_{DOC}$$

$$\frac{d[O_2]}{dt} = \mathbf{Tr}_{O_2} + \mathbf{E}_{O_2} - \mathbf{R}_{OxCarb} - 2{\cdot}\mathbf{R}_{Nit} - 2{\cdot}\mathbf{R}_{SOx}$$

$$\frac{d[NO_3^-]}{dt} = \mathbf{Tr}_{NO_3^-} - 0.8\ \mathbf{R}_{DenCarb} + \mathbf{R}_{Nit}$$

$$\frac{d[Sal]}{dt} = \mathbf{Tr}_{Sal}$$

$$\frac{d[\sum NH_4^+]}{dt} = \mathbf{Tr}_{\sum NH_3} + \mathbf{E}_{NH_3} + \mathbf{R}_{Ox} + \mathbf{R}_{Den} + \mathbf{R}_{SRed} - \mathbf{R}_{Nit}$$

$$\frac{d[\sum HSO_4^-]}{dt} = \mathbf{Tr}_{\sum HSO_4^-} - \frac{1}{2}\mathbf{R}_{SRedCarb} + \mathbf{R}_{SOx}$$

$$\frac{d[\sum H_2S]}{dt} = \mathbf{Tr}_{\sum H_2S} + \frac{1}{2}\mathbf{R}_{SRedCarb} - \mathbf{R}_{SOx}$$

$$\frac{d[\sum CO_2]}{dt} = \mathbf{Tr}_{\sum CO_2} + \mathbf{E}_{CO_2} + \mathbf{R}_{OxCarb} + \mathbf{R}_{DenCarb} + \mathbf{R}_{SRedCarb}$$

$$\frac{d[\sum B(OH)_3]}{dt} = \mathbf{Tr}_{\sum B(OH)_3}$$

$$\frac{d[\sum HF]}{dt} = \mathbf{Tr}_{\sum HF}$$

$$\frac{d[TA]}{dt} = \mathbf{Tr}_{TA} + \mathbf{E}_{NH_3} + \mathbf{R}_{Ox} + 0.8\ \mathbf{R}_{DenCarb} + \mathbf{R}_{Den} + \mathbf{R}_{SRed} + \mathbf{R}_{SRedCarb} - 2{\cdot}\ \mathbf{R}_{Nit} - 2{\cdot}\mathbf{R}_{SOx}$$

BGD
5, 83–161, 2008

Table 6. Monitoring stations on the Scheldt estuary (Westerschelde: "WS"). Coordinates are WGS84 values.

station ID	station name	river km	latitude	longitude
WS1	SSvH Breskens	104	51°24′75″ N	3°34′00″ E
WS2	W5 Sloehaven	96.3	51°26′40″ N	3°40′00″ E
WS3	Borssele	93.0	51°25′50″ N	3°42′40″ E
WS4	W20 Terneuzen	80.0	51°20′90″ N	3°49′60″ E
WS5	Boei 10 Hoedekenskerke	68.1	51°25′10″ N	3°55′30″ E
WS6	Hansweert	60.5	51°26′35″ N	4°01′00″ E
WS7	Waarde	57.7	51°25′62″ N	4°02′10″ E
WS8	Perkpolder	56.7	51°24′01″ N	4°02′27″ E
WS9	Baalhoek	51.8	51°22′31″ N	4°05′30″ E
WS10	Bath	46.1	51°23′54″ N	4°12′29″ E
WS11	Zandvliet	35.3	51°20′72″ N	4°15′56″ E
WS12	Lillo	29.2	51°17′85″ N	4°17′18″ E
WS13	Boei 105 – Punt van Melsele	21.5	51°15′05″ N	4°19′37″ E
WS14	Antwerpen	13.2	51°13′40″ N	4°23′74″ E
WS15	Hoboken	6.1	51°10′60″ N	4°19′66″ E
WS16	Rupelmonde	0.0	51°07′58″ N	4°18′64″ E

BGD
5, 83–161, 2008

Table 7. Budget for $[\sum NH_4^+]$; values in mmol-N m^{-3} y^{-1}; percentages are of total production (positive quantities) or consumption (negative quantities), respectively.

	km 0		km 60		km 104	
$\sum$ prod	4730.9		113.5		146.3	
$\sum$ cons	−4749.6		−123.0		−147.5	
$\mathbf{R}_{Nit}$	−4721.4	99 %	−121.0	98 %	−42.0	28%
$\mathbf{Tr}_{\sum NH_4^+}$	3178.9	67 %	79.5	70 %	−102.7	70%
$\mathbf{R}_{Ox}$	934.5	20 %	31.7	28 %	137.5	94%
$\mathbf{R}_{Den}$	586.8	12 %	2.1	2 %	6.0	4%
$\mathbf{R}_{SRed}$	30.7	1 %	0.2	0 %	2.8	2%
$\mathbf{E}_{NH_3}$	−28.2	1 %	−2.0	2 %	−2.8	2%

Table 8. Budget for $[\sum CO_2]$; values in mmol-C m^{-3} y^{-1}; percentages are of total production (positive quantities) or consumption (negative quantities), respectively.

	km 0		km 22		km 48	
$\sum$ prod	7805.5		5994.9		2503.6	
$\sum$ cons	−7809.4		−6118.7		−2807.1	
$\mathbf{E}_{CO_2}$	−7809.4	100%	−6118.7	100%	−2807.1	100%
$\mathbf{Tr}_{\sum CO_2}$	1481.1	19%	4052.1	68%	2132.1	85%
$\mathbf{R}_{OxCarb}$	3807.8	49%	1526.1	25%	340.9	14%
$\mathbf{R}_{DenCarb}$	2391.3	31%	397.2	7%	28.7	1%
$\mathbf{R}_{SRedCarb}$	125.3	2%	19.5	0%	1.9	0%
	km 60		**km 67**		**km 104**	
$\sum$ prod	479.0		584.5		610.2	
$\sum$ cons	−655.3		−700.6		−610.4	
$\mathbf{E}_{CO_2}$	−655.3	100%	−700.6	100%	−338.2	55%
$\mathbf{Tr}_{\sum CO_2}$	301.6	63%	427.2	73%	−272.2	45%
$\mathbf{R}_{OxCarb}$	165.2	34%	146.9	25%	573.4	94%
$\mathbf{R}_{DenCarb}$	11.0	2%	9.2	2%	25.2	4%
$\mathbf{R}_{SRedCarb}$	1.1	0%	1.1	0%	11.7	2%

BGD
5, 83–161, 2008

Table 9. Budget for $[O_2]$; values in mmol-O_2 m^{-3} y^{-1}; percentages are of total production (positive quantities) or consumption (negative quantities), respectively.

	km 0		km 18		km 48	
$\sum$ prod	13190.2		7123.8		3097.8	
$\sum$ cons	−13255.3		−7163.7		−3038.2	
$\mathbf{E}_{O_2}$	8766.8	66%	7117.4	100%	3097.8	100%
$\mathbf{Tr}_{O_2}$	4423.5	34%	6.4	0%	−1947.1	64%
$-\mathbf{R}_{OxCarb}$	−3807.8	29%	−1817.9	25%	−340.9	11%
$-2\ \mathbf{R}_{Nit}$	−9442.8	71%	−5321.4	74%	−746.6	25%
$-2\ \mathbf{R}_{SOx}$	−4.8	0%	−24.4	0%	−3.6	0%
	km 60		km 67		km 104	
$\sum$ prod	739.4		804.7		640.0	
$\sum$ cons	−716.7		−794.1		−657.9	
$\mathbf{E}_{O_2}$	739.4	100%	804.7	100%	157.3	25%
$\mathbf{Tr}_{O_2}$	−307.7	43%	−474.0	60%	482.7	75%
$-\mathbf{R}_{OxCarb}$	−165.2	23%	−146.9	19%	−573.4	87%
$-2\ \mathbf{R}_{Nit}$	−242.1	34%	−171.5	22%	−84.0	13%
$-2\ \mathbf{R}_{SOx}$	−1.7	0%	−1.6	0%	−0.6	0%

Table 10. Budget for $[NO_3^-]$; values in mmol-N m^{-3} y^{-1}; percentages are of total production (positive quantities) or consumption (negative quantities), respectively.

	km 0		km 60		km 104	
$\sum$ prod	4721.4		121.0		42.0	
$\sum$ cons	−4696.0		−202.8		−71.8	
$\mathbf{Tr}_{NO_3^-}$	−2782.9	59%	−194.0	96%	−51.7	72%
$-0.8\,\mathbf{R}_{DenCarb}$	−1913.0	41%	−8.8	4%	−20.1	28%
$\mathbf{R}_{Nit}$	4721.4	100%	121.0	100%	42.0	100%

Table 11. Volume integrated budgets for $\sum NH_4^+$, $\sum CO_2$, O_2, and NO_3^-; values in Mmol-N (river km)$^{-1}$ y^{-1}.

		km 0	km 18	km 22	km 48	km 60	km 67	km 104
$\sum NH_4^+$	$\sum$ prod	18.9	10.9	9.9	8.0	4.8	4.4	11.1
	$\sum$ cons	−19.0	−11.1	−10.1	−8.6	−5.2	−4.7	−11.2
$\sum CO_2$	$\sum$ prod	31.2	25.9	26.4	56.6	20.2	31.3	46.5
	$\sum$ cons	−31.2	−26.3	−27.0	−63.5	−27.6	−37.5	−46.5
O_2	$\sum$ prod	52.8	29.5	30.6	70.1	31.2	43.1	48.8
	$\sum$ cons	−53.0	−29.7	−30.7	−68.7	−30.2	−42.5	−50.1
NO_3^-	$\sum$ prod	18.9	11.0	10.1	8.4	5.1	4.6	3.2
	$\sum$ cons	−18.8	−10.9	−10.0	−10.2	−8.6	−8.5	−5.5

Table 12. CO_2 export to the atmosphere ($-\mathbf{E}_{CO_2}$) in Gmol y^{-1} per modelled area, $[CO_2]$ and $[CO_2]_{sat}$ are volume and yearly averaged values for the whole estuary in mmol m^{-3}.

	2001	2002	2003	2004
CO_2 export	4.90	3.82	3.08	2.54
$[CO_2]$	62.28	49.23	47.45	40.95
$[CO_2]_{sat}$	17.97	17.62	17.60	17.33
% CO_2 saturation	347	279	270	236

Table 13. Trends in denitrification from the seventies to our model time period.

decade	′70	′80	′00
Gmol N y^{-1} imported into the Scheldt	3.7	4.7	2.4
% of total N lost to the atmosphere	40	23	8
Gmol N y^{-1} exported to the North Sea	1.9	3.6	2.3

Table 14. Export of CO_2 to the atmosphere ($-\mathbf{E}_{CO_2}$) in $Gmol\,y^{-1}$, integrated over our model area.

reference	value
Frankignoulle et al. (1998)	14.5
Gazeau et al. (2005)	11.3
Hellings et al. (2001)	8.2
Vanderborght et al. (2002)	6.8
this study	3.6

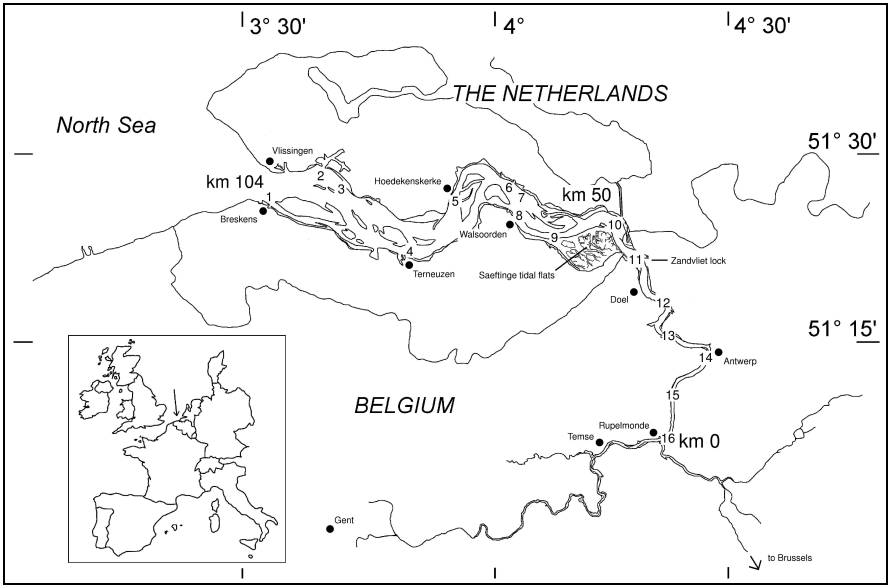

Fig. 1. The Scheldt estuary – monitoring stations WS1 to WS16 are indicated with numbers.

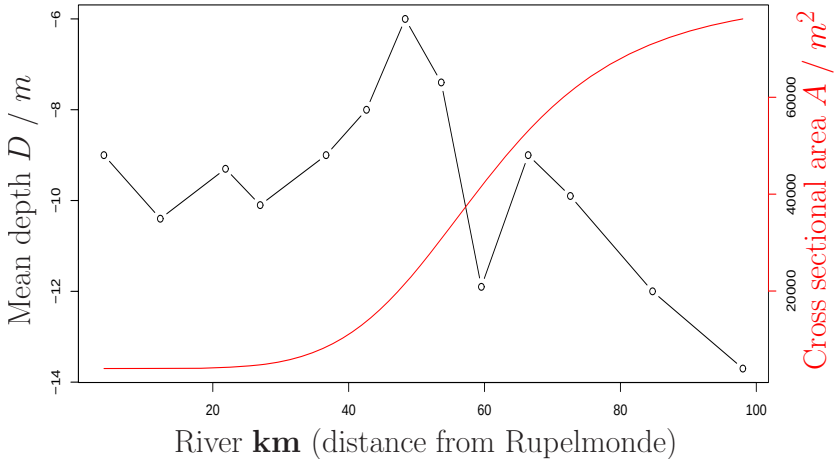

Fig. 2. Mean depth D (black broken line) and cross sectional area A (red solid line) of the Scheldt estuary.

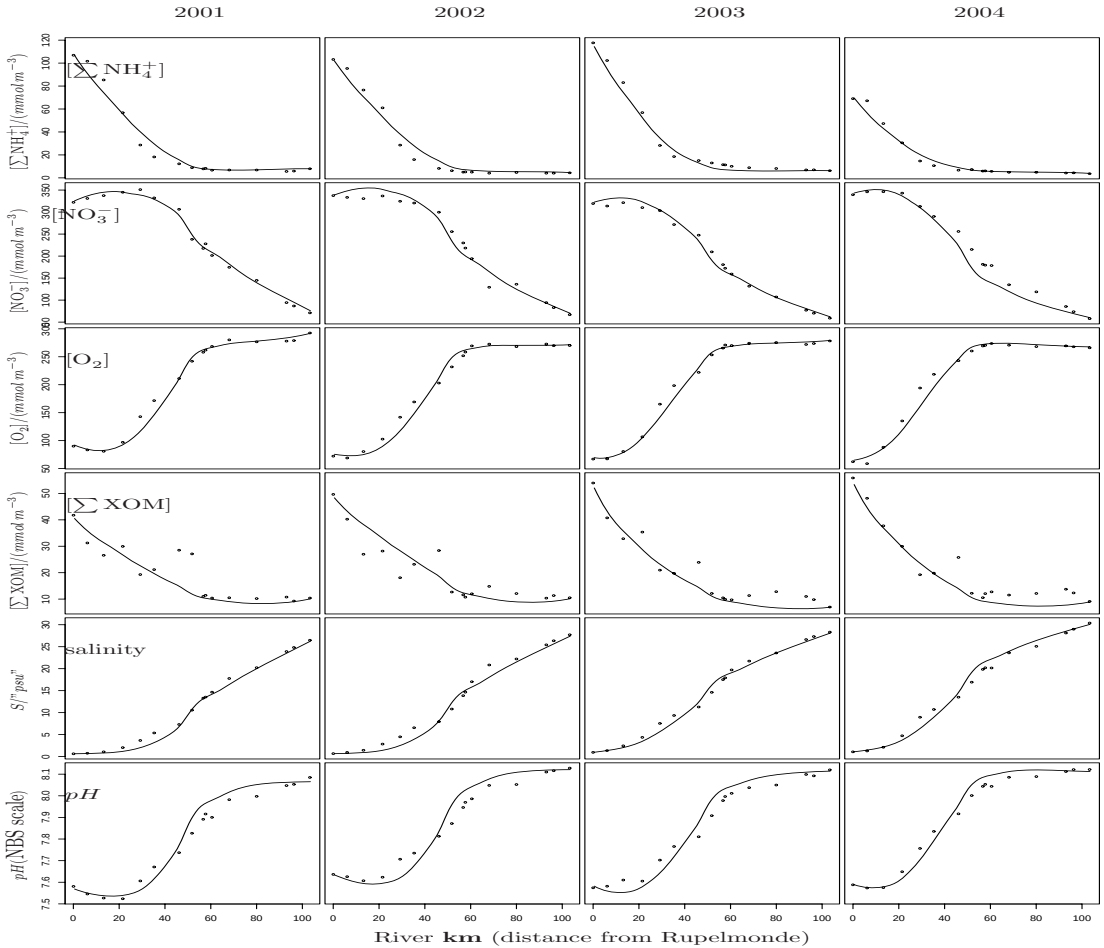

Fig. 3. Fit of the biogeochemical model for 4 consecutive years. Calibration was done on data for 2003 only. Data and model output are yearly averages.

BGD
5, 83–161, 2008

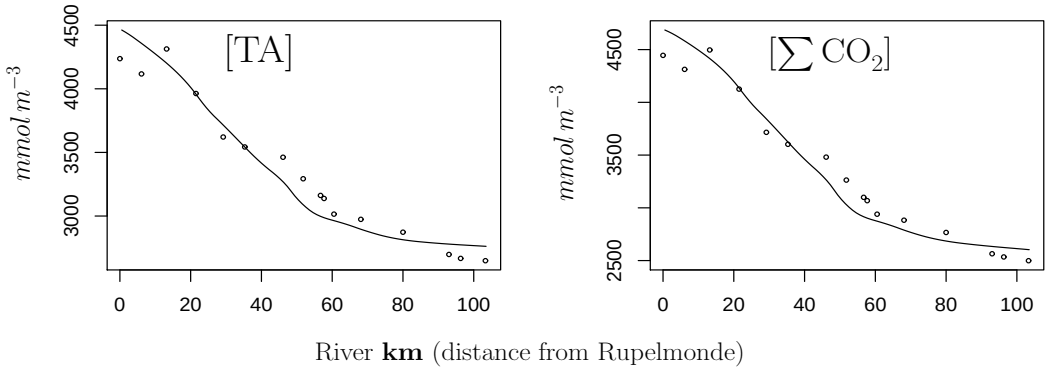

Fig. 4. Yearly averaged [TA] and $[\sum CO_2]$ (model output, 2003) vs. field data provided by Frederic Gazeau (pers. comm. and Gazeau et al., 2005). [TA] data are measurements, $[\sum CO_2]$ data are consistently calculated using conditions of the model.

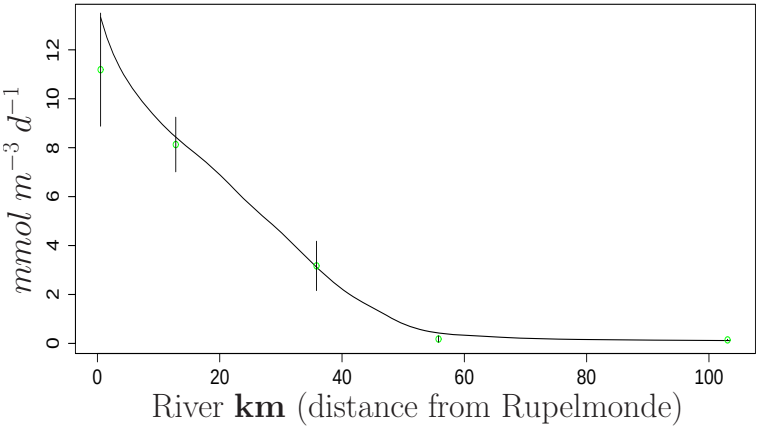

Fig. 5. Yearly averaged $\mathbf{R}_{\mathrm{Nit}}$ (model output, 2003) vs. field data (Andersson et al., 2006).

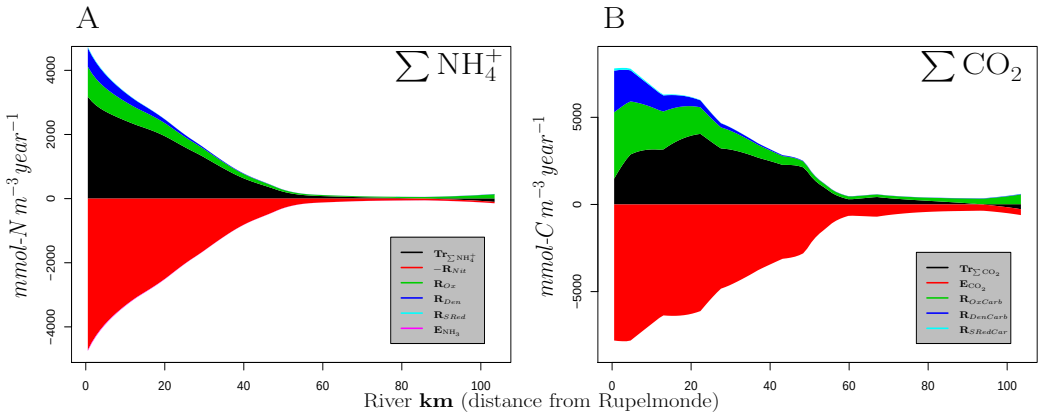

Fig. 6. Budgets for $[\sum NH_4^+]$ **(A)** and $[\sum CO_2]$ **(B)** along the estuary, averaged over 2001–2004 (cumulatively plotted); Values are in mmol m^{-3} y^{-1}.

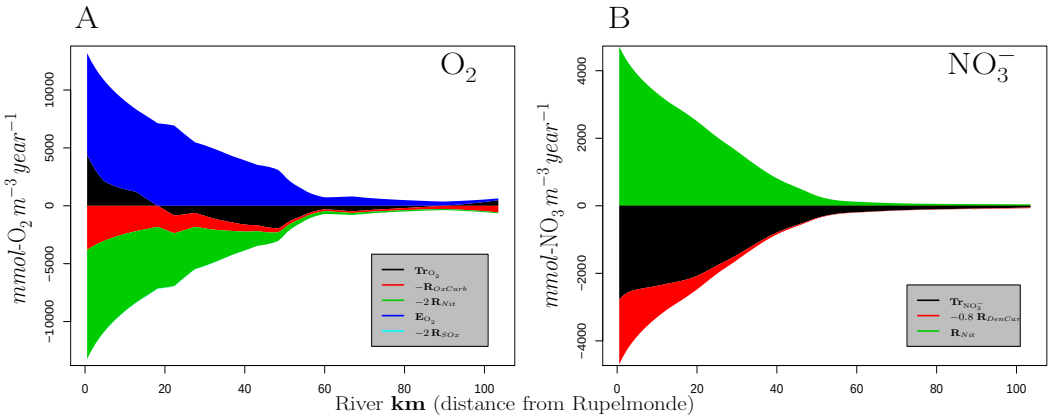

Fig. 7. Budgets for $[O_2]$ **(A)** and $[NO_3^-]$ **(B)** along the estuary, averaged over 2001–2004 (cumulatively plotted); Values are in mmol m^{-3} y^{-1}.

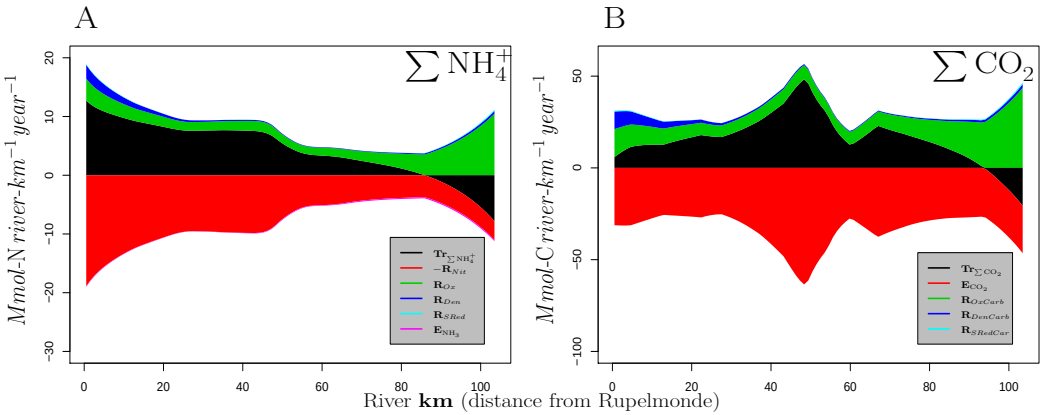

Fig. 8. Volume integrated budgets for $\sum NH_4^+$ **(A)** and $\sum CO_2$ **(B)** along the estuary, averaged over 2001–2004; Values are in Mmol (river km)$^{-1}$ y^{-1}.

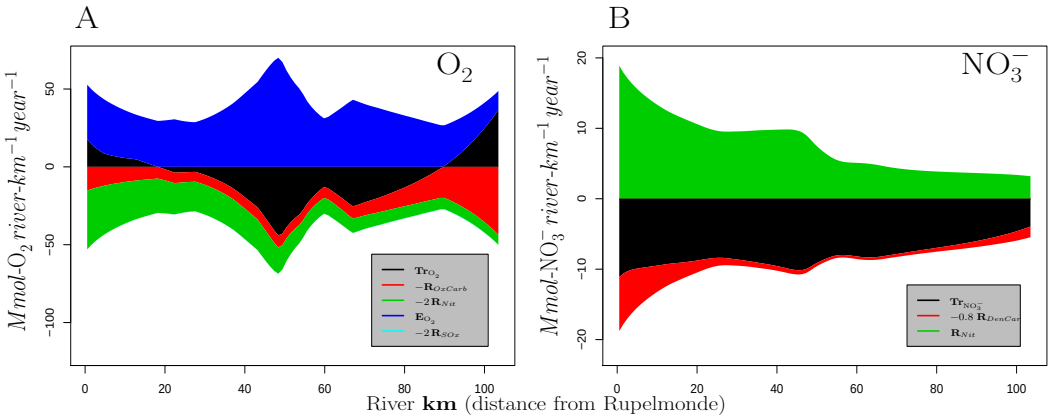

Fig. 9. Volume integrated budgets for O_2 **(A)** and NH_3^- **(B)** along the estuary, averaged over 2001–2004; Values are in Mmol-N km^{-1} y^{-1}.

BGD
5, 83–161, 2008

EGU

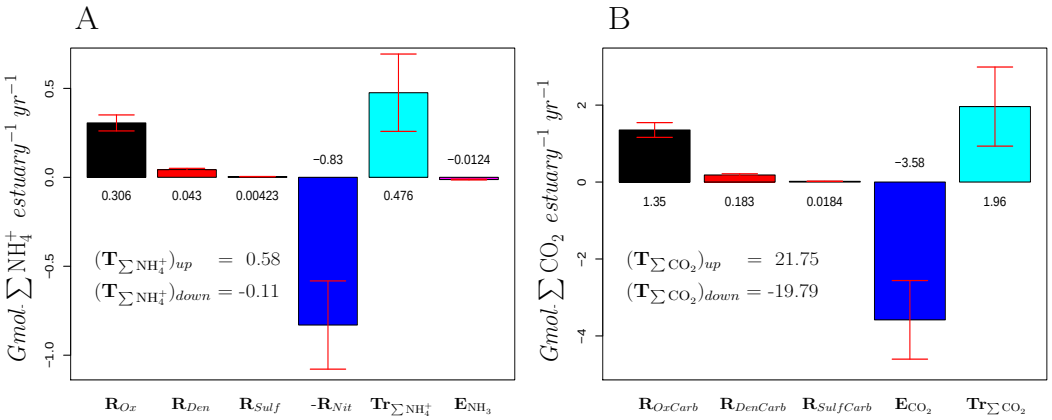

Fig. 10. Total annual budgets for $\sum NH_4^+$ **(A)** and $\sum CO_2$ **(B)** for the whole estuary, averaged over 2001–2004. $(\mathbf{Tr}_x)_{up}$ and $(\mathbf{Tr}_x)_{down}$ signify advective-dispersive import or export at the upstream and downstream boundary. The error bars give the standard deviation σ, obtained from the four model years.

BGD
5, 83–161, 2008

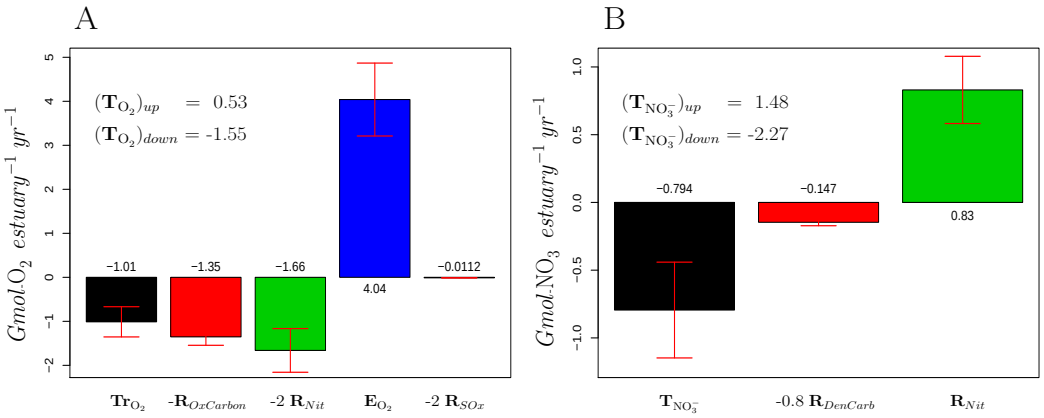

Fig. 11. Total annual budgets for O_2 **(A)** and NH_3^- **(B)** for the whole estuary, averaged over 2001–2004. $(\mathbf{Tr}_x)_{up}$ and $(\mathbf{Tr}_x)_{down}$ signify advective-dispersive import or export at the upstream and downstream boundary. The error bars give the standard deviation, σ obtained from the four model years.

BGD
5, 83–161, 2008

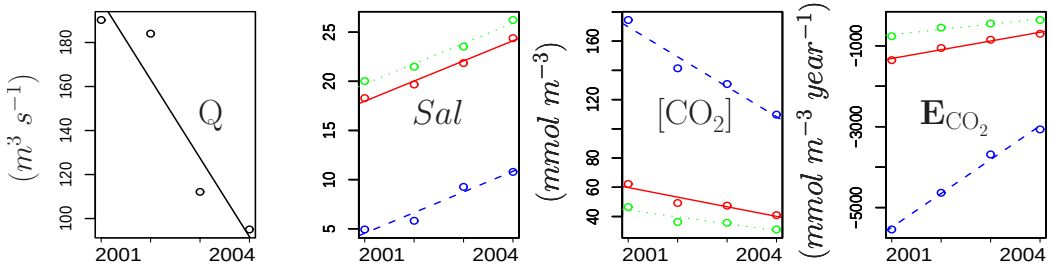

Fig. 12. Trends in key quantities from 2001 to 2004 (*Q* signifies the freshwater flow at the upstream boundary; Sal, $[CO_2]$, $\mathbf{E}_{CO_2}$: volume averaged, solid line: total estuary, dashed line: upper part (to box 50), dotted line: lower part).

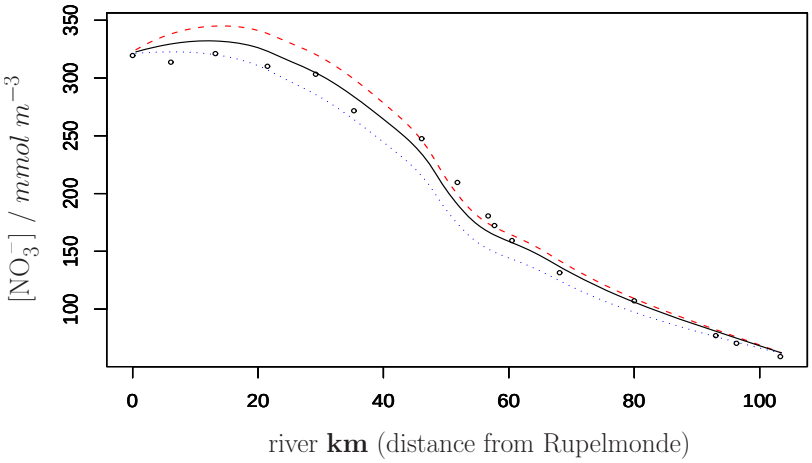

Fig. 13. $[NO_3^-]$ fit with different denitrification parametrisations.

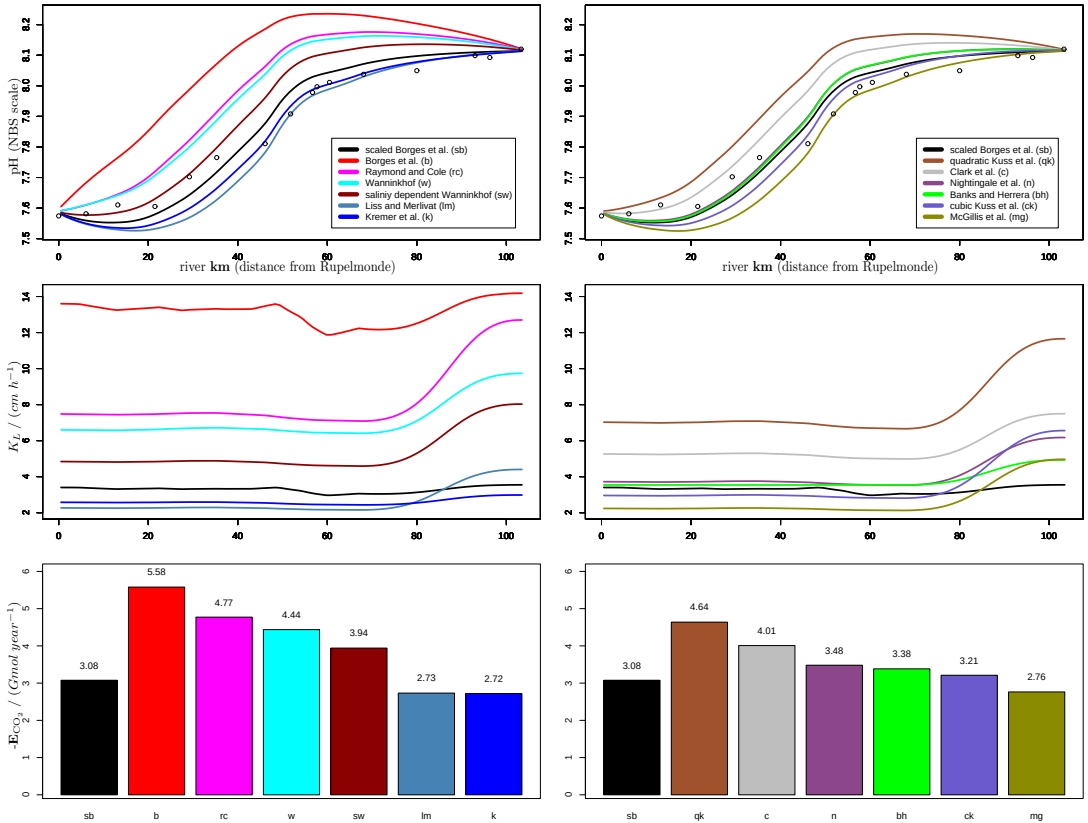

Fig. 14. pH fit, K_L values and -$\mathbf{E}_{CO_2}$ for 2003 for different piston velocity formulations. References: sb: Borges et al. (2004b) scaled with s_{pist} = 0.25; b: Borges et al. (2004b); rc: Raymond and Cole (2001); w: Wanninkhof (1992); sw: Wanninkhof (1992) made salinity dependent by linear interpolation; lm: Liss and Merlivat (1986); k: Kremer et al. (2003); qk: Kuss et al. (2004) quadratic version; c: Clark et al. (1995); n: Nightingale et al. (2000); bh: Banks and Herrera (1977); ck: Kuss et al. (2004) cubic version; mg: McGillis et al. (2001).

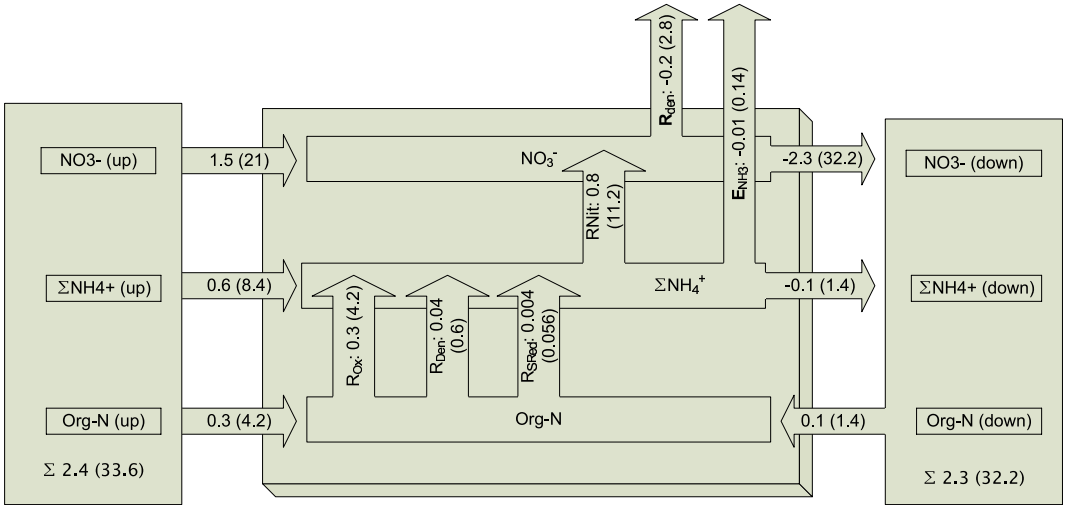

Fig. 15. Tentative nitrogen budget per year over the whole model area, averaged over 2001 to 2004. Values are given in Gmol y^{-1} and in Mt-N y^{-1} (in brackets). Note that the budget is not fully closed, there is an overall loss term of 0.1 Gmol-N y^{-1}. This is consistent with the temporal downward trend in $[\sum NH_4^+]$ and $[NO_3^-]$. Note also that organic nitrogen (Org-N) refers to particulate organic matter (OM). Dissolved organic nitrogen (DON) is not shown in this budget. Using γ_{DOM} and conservatively modelled [DOC], one can estimate that around 0.16 Gmol of DON enters and leaves the estuary on average per year.

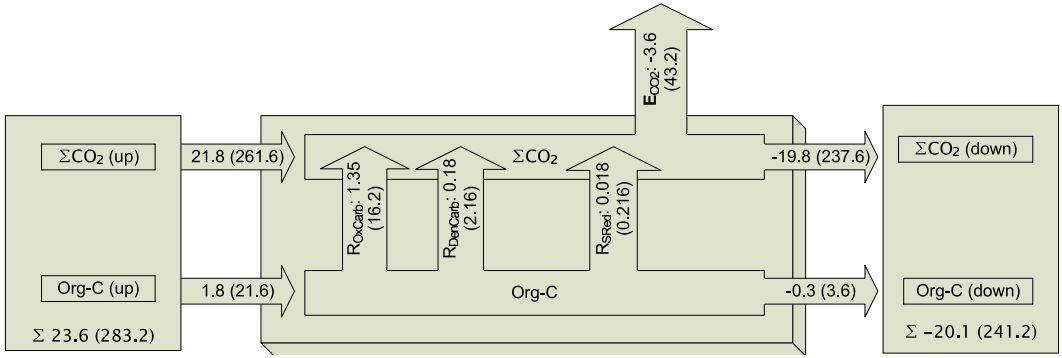

Fig. 16. Tentative carbon budget per year over the whole model area, averaged over 2001 to 2004. Values are given in Gmol y^{-1} and in Mt-C y^{-1} (in brackets). Note that the budget is not fully closed. There is an overall loss term of 0.1 Gmol-C y^{-1}. This is consistent with the temporal downwards trend in $[\sum CO_2]$. Note also that organic carbon (Org-C) refers to particulate organic matter (OM). Dissolved organic carbon (DOC) is not shown in this budget. Around 2.2 Gmol of conservatively modelled DOC enters and leaves the estuary on average per year.